PDC Bit Hydraulic and Mud Rheological Simulation to Model Pressure Drop across Bit

by

Ong Kai Sheng
16325

Dissertation submitted in partial fulfilment of
the requirements for the
Bachelor of Engineering (Hons)
Mechanical Engineering.

January 2016

Universiti Teknologi PETRONAS
Bandar Seri Iskandar
31750 Tronoh
Perak Darul Ridzuan
Malaysia

Certification of Approval

PDC Bit Hydraulic and Mud Rheological Simulation to Model Pressure Drop across Bit

by

Ong Kai Sheng
16325

A project dissertation submitted to the
Mechanical Engineering Program
Universiti Teknologi PETRONAS
in partial fulfillment of the requirement for the
Bachelor of Engineering (Hons)
Mechanical Engineering.

Approved by,

_____

(Dr. Tamiru Alemulemma)

Universiti Teknologi PETRONAS
Tronoh, Perak
January 2016

Certification of Originality

This is to certify that I am responsible for the work submitted in this project, that the original work is my own except as specified in the references and acknowledgements, and that the original work contained herein have not been undertaken or done by unspecified sources or persons.

_____

Ong Kai Sheng

Abstract

When fluid flow from larger into smaller diameter pipes, it experiences a drop in pressure. High pressure drop across bit is an indication of high energy loss in the hydraulic system and also a setback to ROP performance. This is inefficient and pressure pumps would have to be of bigger sizing to make up for the losses. Present form of pressure drop models are in terms of mud density, flow rate, and total flow area. No study on mud rheological parameters specifically the Yield Stress, Consistency Index, and Power Index have been done with respect to pressure drop across bit. The objective of this research is focused on the analysis of CFD simulation and to propose optimized parameters for improved ROP. Single phase flow study of Yield Power Law mud rheology was simulated at bottom hole of horizontal section. For accuracy of simulated results, a mesh independence test was carried out to justify the validity of the simulated results. Preliminary simulation on Yield Power Law Muds showed about 50% reduction of pressure drop across bit as flow rate increase. Parametric study on mud rheology was carried in Design of Experiment. Design points of DOE were sampled mostly using Latin Hypercube Sampling and a few by Central Composite Design. It is found that Kriging in Response Surface study generated the best regression model where the predicted values are closest to the observed values and Kriging has the lowest Maximum Relative Residual (0.000336%). Inlet velocity and Power Index have significant effect on pressure drop. Consistency Index showed moderate effect while Yield Stress showed small effect to pressure drop. This research has 4 input parameters and optimization analysis were done individually where the other 3 input parameters are kept at average values. Optimized parameters are (Inlet velocity = 2.5m/s, Yield Stress = 11.25Pa, Consistency Index = 2.5Pa.s^n, and Power Index = 0.4). This research has proven that pressure loss model should take into account of mud rheology. Further research can be done with PDC bit rotation and its effect on mud behavior. Future work also can include the development of pressure drop model in terms of Mud Density, Total Flow Area, Nozzle Coefficient, Flow Rate, Yield Stress, Consistency Index, and Power Index.

Acknowledgement

The author expresses high level of gratitude and regards to his supervisor, Dr Tamiru Alemulemma, Senior Lecturer of the Mechanical Engineering of UTP. He has provided clear guidance and unwavering support with vast and valuable knowledge. These has helped the author in achieving all required results for this final year project.

The author also expresses his profound gratitude to Universiti Teknologi PETRONAS for providing the facilities and platform for the project. Resource Information Centre (RIC), also known as library, has provided access to hardcopy textbooks. Moreover, the author is given free access to websites containing softcopy full-text scientific database offering journal articles and book chapters. Besides that, UTP has also provided high speed internet browsing experience with speeds up to 8 Mbps. This allows the author to download journals articles and book chapters in a jiff.

Last but not least, the author would like to express many thanks to all the unsung Youtubers who have created video tutorials on simulation software and many more.

Thank you.

Table of Contents

List of Figures

List of Tables

Abbreviations and Nomenclatures

$\vec{F}$	External Forces
$\dot{\gamma}$	Shear Rate
$\bar{\bar{\tau}}$	Stress Tensor
μ	Molecular Viscosity
μ_p	Plastic Viscosity
AADE	American Association of Drilling Engineers
BS	Bit Size
CAD	Computer Aided Design
C_d	Coefficient Of Bit Nozzles
CFD	Computational Fluid Dynamics
C_t	Ratio of Velocity of Particles to the Velocity of Fluid in the Annulus
D	Bit Diameter
DOE	Design of Experiment
ECD	Equivalent Circulating Density
ERD	Extended Reach Drilling
ft/hr	Feet per Hour
ft/s	Feet per Second
FYP	Final Year Project
gpm	Gallons per Minute
HH:MM	Hour:Minute
HHP_b	Hydraulic Horse Power at bit
HIS	Hydraulic Horse Power per Inch Square
hp	Horse Power
h_t	Hydraulic Factor
IADC	International Association of Drilling Contractors
in.	Inch
JSA	Junk Slot Area
K	Consistency Index
lb/gal	Pounds per Gallon
lb/in^2	Pounds per Inch Square
m/s	Meters per Second

MMH	Mixed Metal Hydroxide
MW	Mud Weight
n	Behaviour Index
OBM	Oil Based Mud
PDC	Polycrystalline Diamond Compact
PV	Plastic Viscosity
Q	Flow Rate
Q_{min}	Minumum Flow Rate
RIC	Resource Information Centre
ROP	Rate of Penetration
RPM	Rotations per Minute
SBM	Synthetic Based Mud
SPE	Society of Petroleum Engineers
t	Time
TFA	Total Flow Area
UTP	Universiti Teknologi PETRONAS
V_a	Velocity of Fluid Flow in Annulus
Vin	Velocity at Bit Nozzles
V_p	Velocity of Particles
WBM	Water Based Mud
WOB	Weight on Bit
YP	Yield Point
YPL	Yield Power Law
ΔP_b	Pressure Drop Across Bit Nozzles
ρ	Density
$\rho\,\vec{g}$	Gravitational Body Force
τ	Shear Stress
τ_y	Yield Stress
υ	Velocity
$\mathcal{I}$	Identity Unit Tensor
R_1, R_2, R_3	Constants
p	Static Pressure

Chapter 1: Introduction

1.1 Background of Study

In the oil and gas industry, drilling cost and time are of major concerns. Operators of this field have their focuses centered on minimizing the overall drilling cost while maintaining safe practices and environmental friendly operations. Rate of Penetration (ROP) is a measure of drilling speed. Based on the relationship between drilling cost and ROP, it had been shown that maximizing the ROP will result in minimizing the drilling cost [1].

Studies have been done on factors affecting ROP. These factors are categorized into bit design parameters and operational parameters. Bit design parameters significantly affecting ROP are Junk Slot Area (JSA) and Bit Size (BS). Operational parameters are Weight on Bit (WOB), Rotation of drill bit (RPM), Hydraulic Horsepower (HHPb), Flow Rate, Nozzle Size, and Mud Weight (MW) [2].

High ROP would generate high rate of cuttings and vice versa. The removal of cuttings is undeniably necessary so that the bit can be in direct contact with bottom hole formation and drill deeper and faster. Cuttings are removed as mud circulates to the top and carries the cuttings along. When cuttings accumulate at bottom hole, Equivalent Circulating Density (ECD) increases and ROP decreases.

Besides that, bit hydraulics plays an important role during drilling. Good bit hydraulics help jet through the formation, keep the PDC cutters cool and clean, and prevents the JSA and nozzles from clogging up and balling.

Moreover, mud rheology plays a huge role in drilling as well. Two main mud properties that have direct impact to removal of cuttings are viscosity and gel strength. Mud viscosity and gel strength primarily suspense cuttings and effectively sweeps the cuttings out of hole.

1.2 Problem Statement

During drillings, bit hydraulics is crucial for the removal of cuttings and cutting the PDC cutters. With poor bit hydraulics, PDC bit may face problems like bit balling and plugged nozzle. These phenomena are the obstruction of JSA and nozzles which are caused by poor cuttings removal away from the PDC bit. On the other hand of the spectrum, when bit hydraulics is extreme, PDC bit may have its matrix body worn away by erosion. PDC cutters may loss at bottom hole when matrix body around PDC cutters get eroded away. Improper and unbalanced cooling rate of bit hydraulics also lead to heat checking of the PDC cutters.

Additionally, poor cuttings removal leads to circulation of cuttings at bottom hole and it increases the Equivalent Circulating Density (EDC) of drilling fluid. When the ECD becomes too high, annulus pressure also increases to a point where it is higher than the wellbore pressure and this leads to possible lost circulation and well premature fracture. Oil and gas may gush out upon the premature fracturing and this is not favorable in midst of drilling.

Furthermore, there are limits to studies through experimental setup. Limits are such as parametric study, procurement of materials, and scale of experiment. Unlike experimental setup, Computational Fluid Dynamics (CFD) is able to overcome these aforementioned limits. In a virtual environment, the scale of simulation can be true to size and the environmental parameters can be kept constant. Properties of material can be manipulated easily through inputs. Most importantly, results can be analyzed easily and more accurately.

High pressure drop across bit nozzles is an indication of energy loss in the hydraulic system. It is inefficient and the pressure pumps have to be of bigger sizing to make up for the losses. How does mud rheology affect pressure drop across bit nozzles?

1.3 Objectives

The objectives of this project are:

- To develop a CAD and CFD model for a typical PDC bit.
- To develop regression models for the pressure loss around the PDC bit.
- To analyze the CFD simulation result and propose optimized parameters for improved ROP.

1.4 Scope of study

The scopes of study based on the objectives can be simplified as follows:

- PDC bit size of 8.5 inches with length of CAD model 5 times the diameter of PDC bit.
- Single phase flow.
- Flow rate: 100 to 1000 gpm
- Mud rheological parameters (Yield Stress, Consistency Index, and Power Index).

To simplify the numerical functions, limitations will be implemented as below:

- PDC bit instead of roller-cone bit as roller-cone bit has moving parts.
- PDC bit layout in horizontal section of well.
- Stagnant PDC bit without rotation; neglect WOB and RPM.
- Fixed geometry and design of a typical 8.5 inch PDC bit.
- Length of drill pipe will be 5 times the diameter of PDC bit.
- For a wellbore with deviation greater than 10°, a required minimum liquid-phase annular velocity of 180 to 200 ft/min is recommended [3].
- Minimum flow rate for 8.5 in. PDC bit is 295.62 gpm.
- High hydrostatic pressure above 5,000 psi can induce bit balling issue in water based mud. HSI less than 1.0 hp/in^2 will not be able to clean the bits [4].

Chapter 2: Literature Review

2.1 PDC Drill Bit

Polycrystalline diamond compact (PDC) bits are one of the most important drill bit for oil well drilling. PDC bit is a fixed-head bit where it rotates as a single piece without any mechanical parts as shown in Figure 2.1. Fixed cutters bits are first manufactured in year 1976. With advances in today's technology, PDC bits are gaining popularity amongst operators and PDC bits are now as common as roller-cone bits.

Fixed cutter bit's body is made up of tungsten carbide matrix powder bonded together with a metal alloy binder. This matrix bit body is very resistant to erosion and abrasion. However, a cheaper alternative is milled steel body which sacrifices erosion and abrasion resistance feature.

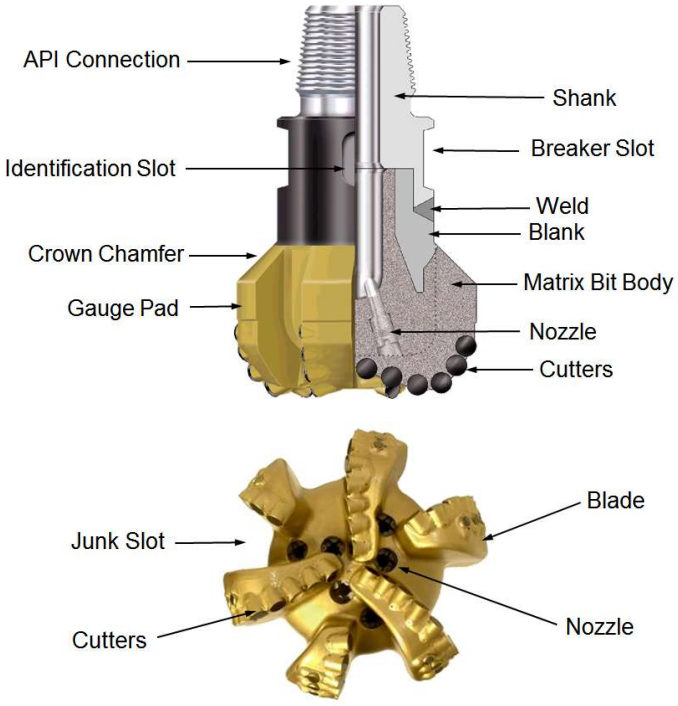

Figure 2.1: PDC bit components with side and top views [5].

PDC bits are highly associated with bit hydraulics during drilling. Below are problems commonly found on PDC bits due to either too poor or too aggressive bit hydraulics.

- Bit Balling and Plugged Nozzle as shown in Figure 2.2: A situation in which cuttings and formation are packed around the cones until they don't rotate or drill forward and the obstruction of the junk slot and nozzles by the cuttings.

Figure 2.2: Bit Balling and Plugged Nozzle [5].

- Erosion and Loss Cutters as shown in Figure 2.3: Loss of carbide substrate behind the diamond table or loss of bit-body material from fluid action and results in complete loss of one or more inserts/cutters, resulting in an empty insert hole.

Figure 2.3: Cutter and matrix bit body erosion and loss of PDC cutter [5].

- Heat Checking as shown in Figure 2.4: Surface cracking of inserts, generally on the outer cutting structure due to bad cooling efficiency of bit hydraulics.

Figure 2.4: Heat Checking of cutter [5].

Besides that, bit hydraulics also causes swab and surge pressures. The higher the flow rate of drilling fluid, the higher the drop in pressure at the bit. Swab pressure is the decrease in pressure at bottom hole which gives drillers hard times to pull the drill string out of hole. Friction between the moving pipes and stationary drilling mud contributes to this phenomenon. The reverse movement of the pipes carries the similar event of change of pressure. When running the pipes in hole, the pressure increases due to movement of the pipes. This is called surge pressure. The swab and surge pressure need to be control so that it doesn't bring about serious problems such as a kick or formation break down.

These above mentioned problems can be avoided with good and optimal bit hydraulics illustrated in Figure 2.5.

Figure 2.5: Illustration of Bit Hydraulics [6].

2.2 Bit Hydraulics

Bit Hydraulics plays important role in cuttings removal away from PDC bit. Poor hydraulics may cause bad cuttings removal away from PDC bit and results in many problems as mentioned earlier.

Optimization of bit hydraulics is through maximizing bit horsepower or nozzle-jet impact force [7]. This brings about effective cuttings removal as the cuttings are removed as fast as they are generated [8].

Flow rate of mud has significant positive effect on cuttings removal away from PDC bit [9-13]. Increasing the annular velocity by increasing the flow rate decreases the cuttings bed height significantly.

At constant mud flow rate, smaller-sized nozzles increase cutting transport velocity as they provide higher jet velocity at bottom hole. Two nozzles showed higher cuttings-transport ratio as compared to three nozzles. This is because the two nozzles generated asymmetrical flow which result in higher jet velocity and improved cutting transport [14]. For a similar total flow area (TFA) of nozzles, higher number of nozzles improves cuttings removal away from PDC bit as more nozzles provide a more-uniform distribution of fluid flow [15].

Bigger face volume of bit is at higher risk of bit balling when drilling at low ROP. And lower face volume achieved maximum ROP without balling. There is no correlation between face volume, JSA, and cuttings removal away from PDC bit efficiency [16].

Besides that, ratio of cuttings velocity to annulus velocity (C_t) and ROP increase as HIS increases. However, C_t is less sensitive to HIS as compared to ROP. C_t is found to be a function of nozzle-jet velocity and showed less sensitivity to number of nozzles, arrangement, and bit waterway profile [17].

The ratio of average velocity of particles to the average fluid velocity in the annulus is C_t and this is an indicator of hydraulics performance of the bit. The value of C_t depends on plane location. If the plane location is at downhole and close to the drill bit, particles would have a higher velocity to annulus fluid velocity. This is due to the high nozzle-

jet velocity at the drill bit. On the other hand, if the plane is away from the drill bit, the value of C_t would be smaller. This is due to particles reaching terminal velocity away from the drill bit.

$$C_t = \frac{V_p}{V_a} \quad \text{(2.1)}$$

Where V_p is average velocity of particles (m/s); V_a is average velocity of fluid flow in annulus (m/s).

Bit hydraulic energy, H_b, is the energy needed to counteract frictional energy (loss) at the bit or can be expressed as the energy expended at the bit:

$$H_b = \frac{P_b Q}{1714} \quad \text{(2.2)}$$

Where H_b is Bit hydraulic energy (hp); P_b is bit nozzle jets pressure loss (lb/in^2); Q is flow rate (gpm)

Minimum flow rate, Q_{min} in terms of bit diameter, D for PDC bits can be calculated through equation below:

$$Q_{min} = 12.72\, D^{1.47} \quad \text{(2.3)}$$

For PDC bit size of 8.5 inch, the calculated minimum flow rate is 295.62 gpm.

2.3 Pressure Drop Across Bit

Pressure drop across a bit happens when mud flows through the bit nozzles. The mud experiences this drop in pressure simply because it moves from large diameter drill pipes into the small diameter bit nozzles. The analogy of pressure loss across bit nozzles illustrated between a constant head flow and a restricted flow as shown in Figure 2.6 and 2.7. The constant head flow shows a steady gradient of pressure drop along a horizontal pipe. On the other hand, the turbine constricted flow in between points E and F shows a sudden drop in pressure across the constriction.

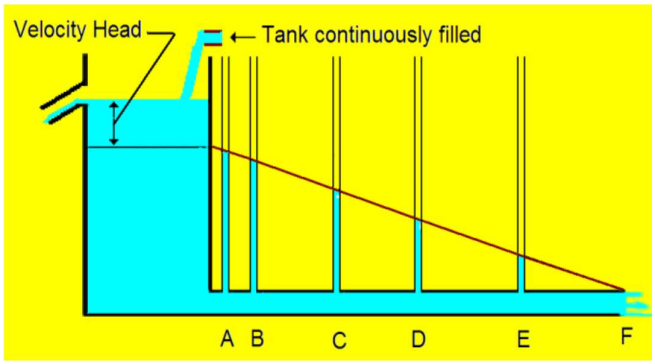

Figure 2.6: Illustration of a constant head flow [18].

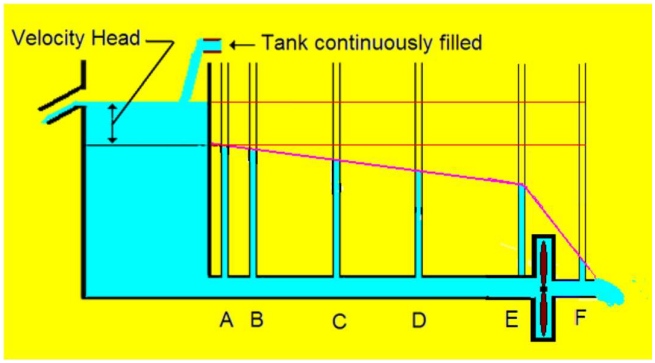

Figure 2.7: Illustration of a turbine constricted flow [18].

This is highly important for the optimization of drilling hydraulic with the objective of maximizing hydraulic horse power or impact force without neglecting effectiveness of cutting removal. This sudden loss of pressure can be calculated from mud weight along with various parameters and can be derived from potential or kinetic energy.

By horse power at bit [19],

$$\Delta P_b = \frac{(1714)(HHP_b)}{Q} \quad \text{(2.4)}$$

By velocity of mud [8],

$$\Delta P_b = \frac{(MW)(V_n{}^2)}{1239} \quad \text{(2.5)}$$

By flow rate, total flow area, and nozzles coefficient [18],

$$\Delta P_b = \frac{(MW)(Q^2)}{12032(C_d{}^2)(TFA^2)} \quad \text{(2.6)}$$

By flow rate, total flow area, rate of penetration, and bit rotation per minute [19],

$$\Delta P_b = \frac{(MW)(Q^2)}{8795[(TFA)(e^{-0.832})(\frac{ROP}{RPM})]^2} \quad \text{(2.7)}$$

Where ΔP_b is bit nozzle jets pressure loss (lb/in^2); HHP_b is horse power at bit (hp); MW is mud weight (lb/gal); V_n is velocity of mud (ft/s); Q is flow rate of mud (gpm); TFA is total flow area of bit nozzles (in^2); C_d is coefficient of bit nozzles (0.95 or 1.00 or 1.03 unitless); ROP is rate of penetration (ft/hr); RPM is drill bit rotation per minute (rpm).

From drill pipe into the bit nozzle, majority of fluid flow transitions from laminar flow to turbulent flow. Due to this, pressure drop is mainly affected by turbulent flow and a small amount of laminar flow. A fully turbulent flow would result in a pressure loss that is proportional to flow rate squared or velocity of mud squared. In 1982, the industry used programs with flow rate exponent ranged from 1.4 to 1.9. This technique is carried out to compensate the fact that the flow is not completely laminar nor turbulent. This compensation translates into nozzle coefficient squared which is added as a denominator as shown in equation 2.6. In essence, this coefficient is used to correct the pressure loss calculation. Although untested, the coefficient is claimed to be a function of mud weight or plastic viscosity [18]. Nozzle coefficient of 1.03 is used for accurate calculation.

2.4 Mud Rheology

Mud type has small to moderate positive effect on cuttings removal away from PDC bit [20]. Different mud types lead to different bed consolidation. Conventionally, there are two types of mud which either oil based or water based mud. Oil based mud and water based mud having the same rheology generally perform the same in cuttings removal away from PDC bit.

The two mud properties that have direct impact on cuttings removal away from PDC bit are viscosity and density. The main functions of density are mechanical borehole stabilization and the prevention of formation-fluid intrusion into the annulus [21]. If density is out of balance, it brings about adverse effect on the ROP and may cause fracturing of the formation. Mud density is not a suitable criterion to optimize cuttings removal away from PDC bit although it increases as number of cuttings particle increases [21]. However, viscosity plays function of the suspension of cuttings which is crucial for cuttings removal away from PDC bit.

Hole-cleaning efficiency and cuttings transport are primarily controlled by liquid-phase velocities and solids concentration. Based on studies and field experiences, the removal of cuttings is more efficient with two-phase fluid. Cuttings bed formation can be minimized with the presence of a turbulent flow regime. The most critical parameter controlling the cuttings transport is liquid velocity. It has been concluded that a minimum liquid-phase annular velocity of 180 to 200 ft/min is required in a wellbore with a deviation greater than 10° [3].

Rheology is defined as the science of deformation and flow of matter [22]. To date, all fluids are classified as either Newtonian or Non-Newtonian. Several rheological models have been developed based on research over time as shown in Figure 2.8.

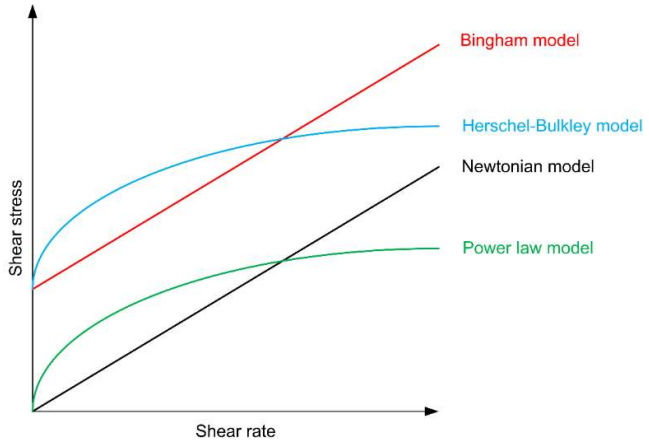

Figure 2.8: Plot showing the most used rheological models in the drilling industry for different fluids [23].

The Newtonian fluid model is valid for fluids that does not change properties during time or shear stress variations, i.e. time independent and consistent. Newtonian fluids have a linear proportional relationship between the shear stress, τ, and the shear rate $\dot{\gamma}$, where μ is the constant of proportionality. In mathematical terms this means:

$$\tau = \mu \dot{\gamma} \quad \text{.....} \quad (2.8)$$

The Bingham plastic model, also known as the Yield Point (YP) model or simply the Bingham model, describes a fluid with a yield stress component and a Newtonian component. The fluids that fit this model require a certain amount of shear stress before flowing. After exceeding the critical stress value, the fluid yields and will thereafter behave as a Newtonian fluid with increasing shear stress. Everyday examples of Bingham fluids are mayonnaise and ketchup. This model also includes fluids that hold solids suspended [24]. τ_y is the yield stress and μ_p is the plastic viscosity. The definition is:

$$\tau = \tau_y + \mu_p \dot{\gamma} \quad \text{.....} \quad (2.9)$$

There are two basic forms of power law fluids, depending on the value of the coefficients in the power law equation, k and n. Pseudoplastic fluids are shear thinning, meaning they will have less viscosity with higher shear rates and behavior index, $n <$ 1. Dilatant fluids are shear thickening, and less common than shear thinning fluids in

nature and behavior index, $n > 1$. k is the consistency index and n is the power law index. Power law fluids are defined as:

$$\tau = k\,\dot{\gamma}^{n} \quad \text{..... (2.10)}$$

The Herschel-Bulkley model is also called the Yield Power Law (YPL) model, since it takes both a yield point and a power law development into account. Effectively, it is a combination of the Bingham and power law fluid models. The Herschel-Bulkley model is often used to describe oil-well drilling fluids, since it considers both a yield point and power law development with increasing shear rate. The yield point factor is due to gelling.

$$\tau = \tau_{y} + k\,\dot{\gamma}^{n} \quad \text{..... (2.11)}$$

The rheological characteristics of drilling mud such as PV and YP and the flow behavior indicates such as k and n, of drilling mud play in an important role in cleaning of drill cuttings. These fluid properties, especially the low shear rate rheological properties that prevail at annular section between the drill pipe and borehole wall have a major impact on the cuttings removal efficiency of drilling mud.

According to experimental data, yield point of drilling mud has favorable effect on the cuttings transport capacity of drilling mud. Increasing the yield point to plastic viscosity ratio increases the carrying capacity in concentric annuli [9]. Increasing apparent viscosity, yield point and initial gel strength increases the carrying capacity in low and medium annular velocity in concentric annuli. Higher n value causes higher lift force. Higher k values for a mud system helps to keep the particles in suspension for longer periods of time. Mud rheology has moderate effect on small cuttings removal away from PDC bit compared to large cuttings. Low viscosity mud is more effective in cuttings transport than high viscosity at the same flow rate.

New generation fluid like foam have high power index, n, at a low shear rate are effective in cuttings removal away from PDC bit. Foam has low variable density that can control the bottom hole pressure. It provides sufficient lifting in transporting cutting. There is no expression to the foam model but foam is typically dependent on foam quality.

Both of the foam and mud have different rheological properties and the author believes it should give some substantial effects on the PDC drill bit since it rotates at different revolution per minute (rpm) at different well depth. This actually improves the foam quality but the cutting efficiency drops as the well deviates from the vertical.

Various mud types and rheological properties from previous studies are tabulated in Table 2.1.

Table 2.1: Mud Types and Rheology.

Name/Type		Quality		Rheology		
		Details	**Weighting agent**	τ_o	k	n
Water Based Mud [25]	WBM A	Polymer	Carbonate	-	12.51	0.15
	WBM B	Bentonite	Barite	3.78	0.446	0.69
	WBM D	MMO-Bentonite	Barite	11.84	0.438	0.7
	WBM F	Polymer	Carbonate	-	4.14	0.21
	WBM G	Polymer-glycol	Barite	-	2.61	0.32
Oil Based Mud [25]	SBM N	Synthetic 80:20	Barite	4.47	0.172	0.76
	OBM P	Mineral 80:20	Barite	0.74	0.041	0.82
Aqueous Foam [26]	70%	-	-	-	0.84	0.45
	80%	-	-	-	1.96	0.4
	90%	-	-	-	3.73	0.36
WBM with Metal Hydroxide [27]	3.3g (2.62%)	Mixed Metal Hydroxide	Carbonate	8.46	0.164	0.669

Where WBM is Water Based Mud; OBM is Oil Based Mud; SBM is Synthetic Based Mud; MMH is Mixed Metal Hydroxide

2.5 Rate of Penetration

Rate of penetration (ROP) is the speed of drilling; the rate of drill bit breaking rocks beneath it. This parameter is highly associated to drilling cost. The higher the ROP, the higher the savings on drilling cost. ROP has moderate negative effect whereby increase in ROP increase hydraulic requirement for effective hole cleaning [10].

The hydraulic effect on drilling rate was modeled based on the major hydraulic parameters which are jet impact force, hydraulic horse power and jet velocity [28]. Exponential fluctuations of ROP was found to be affected by the hydraulic horse power concentration at the bit while other parameters are held constant [29]. High hydraulic energy increases the drilling rate and also lead to better hole cleaning [30]. The new hydraulic model was developed [31] as below:

$$ROP_{actual} = ROP_{clean} * h_t \quad \text{(2.12)}$$

$$h_t = R_1 \frac{(HSI * \frac{JSA}{20})^{R_2}}{ROP_{clean}{}^{R_3}} \quad \text{(2.13)}$$

Where *ROP* is Rate of penetration (m/hr); h_t is Hydraulic factor; *JSA* is Junk slot area (inch^2); *HSI* is Hydraulic horse power per unit area (hp/in^2); R_1, R_2, R_3 are constants.

2.6 Conservation Equations

Mass Conservation Equation

The conservation of mass equation states that the change of mass inside the control volume is equal to the balance of fluid mass entering and leaving the control volume. The conservation principle is represented through the continuity equation:

$$\frac{\partial \rho}{\partial t} + \nabla.(\rho\ \vec{v}) = 0 \quad \text{..... (2.14)}$$

Where ρ is density; υ is velocity; t is time.

The first term is the unsteady term which represents the rate of change of density and the second term is the convective term which represents the net rate of mass flow through the control volume.

Momentum Conservation Equations

The governing equation for the conservation of linear momentum, written in conservative form, is:

$$\frac{\partial}{\partial t}(\rho\ \vec{v}) + \nabla.(\rho\ \vec{v}\vec{v}) = -\nabla p + \nabla.(\bar{\bar{\tau}}) + \rho\ \vec{g} + \vec{F} \quad \text{..... (2.15)}$$

$$\bar{\bar{\tau}} = \mu[\nabla\ \vec{v} + \nabla\ \vec{v}^{T}] - \frac{2}{3}\nabla.\vec{v}\ I \quad \text{..... (2.16)}$$

Where p is the static pressure; $\bar{\bar{\tau}}$ is the stress tensor; $\rho\ \vec{g}$ is gravitational body force; $\vec{F}$ is external forces; μ is the molecular viscosity; I is the identity unit tensor; $\nabla.\vec{v}$ is 0 for incompressible fluid.

The above conservation equations of mass and momentum together comprise the Navier-Stokes equations and are solved for various flow conditions in Fluent.

2.7 Computational Fluid Dynamics (CFD)

Computational Fluid Dynamics (CFD) method are used in the past to study PDC bit Hydraulics. Unlike experimental studies, CFD simulations allow researchers to have more flexibility in terms of various parameters. This brings about more parametric studies carried out under the same time duration between experimental and CFD simulation.

Study on hydraulics performance of PDC bits was done through computational particle tracking simulation as shown in Figure 2.9 & 2.10 [17]. Similarly, parametric study on effect of nozzles towards bit hydraulics was carried out using numerical simulations [32]. Another study was done with numerical simulation on the optimization of TFA and nozzle angle for better bit hydraulics of Bi-Center Bit [33].

Computational Fluid Dynamics (CFD) is a well-recognized technique in the world of research. It always provides an alternative method to research when hindered by limitations of experimental testing. Furthermore, it complements results of experimental testing.

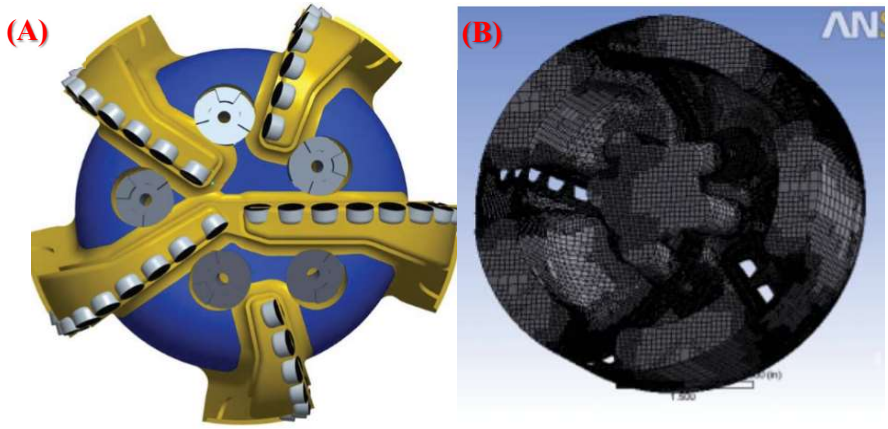

Figure 2.9: (A) Front view of five bladed PDC bit (B) Generated mesh for a section of drill bit fluid volume [17].

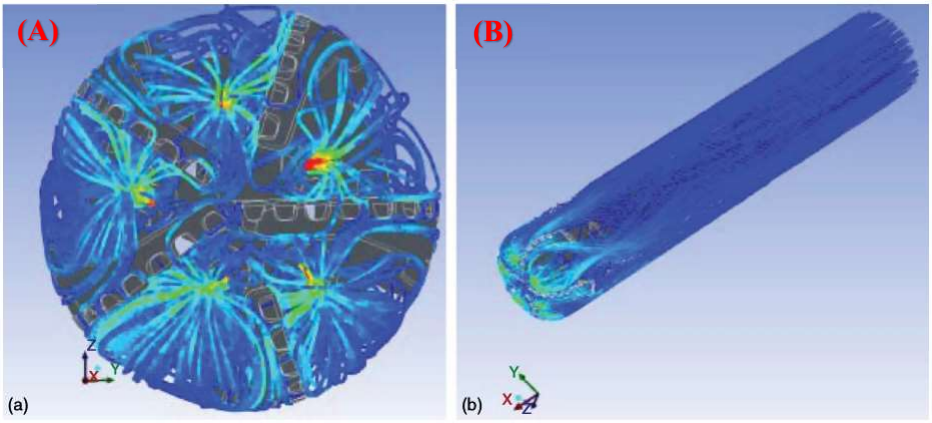

Figure 2.10: (A) Fluid-flow streamlines over face of bit. (B) Particle trajectories in annulus [17].

2.8 Summary

Yield Power Law model will be used to govern various fluid rheology. This research is focused on the effects of single phase flow to bit hydraulics at bottom hole of horizontal section. Mud of different rheology will be used to study the effects on bit hydraulics. For accuracy of simulated results, a mesh independence test will be carried out before parametric studies on PDC bit hydraulics. Multiple runs of simulations will be conducted until the percentage difference between results is less than five percent.

Chapter 3: Methodology

3.1 Introduction

Flow of the major tasks of this project can be layout as blocks in Figure 3.1. First step is to obtain the necessary fundamental equations. Followed by CFD modeling and simulation. Simulation shall be run under various mesh resolutions until percentage error between results of different mesh sizes are not more than five percent. Once the overall method is acknowledged, this project will continue with parametric studies and analysis.

This research is focused on the effects of single phase flow of various mud rheology to bit hydraulics at bottom hole of horizontal section. Mud of different rheology is used to study their effects on bit hydraulics. Fluid viscosity models used is Yield Power Law. This law requires consistency index, power index. Yield stress, and critical shear rate. ANSYS Fluent uses these parameters to determine the viscosity for various muds in Table 2.1. The pressure loss across the bit nozzles is analyzed and a pressure loss regression model is developed.

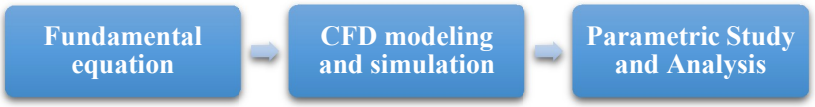

Figure 3.1: Flow of Major Tasks.

3.2 Computer Aided Design Model

To simulate flow around a drill bit at bottom hole, it is required to prepare 2 CAD drawings. A typical drill bit of length and diameter of 1.12m and diameter of 220mm respectively is drawn in ANSYS Modeler. This is followed by a drawing of a borehole of the same length and diameter. Both CAD drawings are then aligned together with the same axial axis. After that, the drill bit is subtracted from the borehole. This leaves an annulus which the mud will flow from drill pipe passing through bit nozzles into

the annulus and then flow away from the bit as shown in Figure 3.2. Length of the model is 1.12m and diameter of 220mm.

Figure 3.2: Visualization of borehole (Brown) subtracts the drill bit (Gold) and leaves annulus.

3.3 Mesh Independency Study Simulations

After the CAD model is prepared, it is necessary to lay mesh on the model as shown in Figure 3.3. The smaller the mesh size, the more accurate the results will be and the longer the time taken for simulation. This calls for mesh independence study which is the optimization of simulations on various mesh sizes ranging from 0.01 to 0.005 element size as tabulated in Table 3.1. For mesh independence study, water is selected with default values of properties for faster simulation time. Once the solver parameters are settled as tabulated in Table 3.2, hybrid initialization method is initialized and followed by the run of calculation. This optimization aims to reduce unnecessary simulation time and produce consistent results. Validity of the results can be justified with small percentage error of less than five percent amongst all convergence criteria.

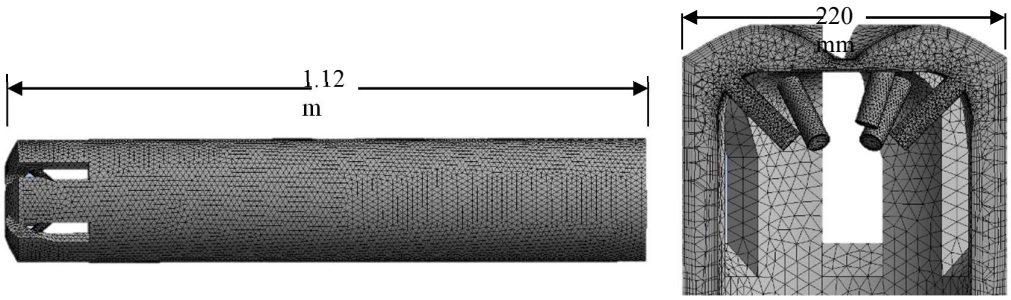

Figure 3.3: Side and Cross-sectioned view of the meshed CAD model.

Table 3.1: Grid size and computation time.

Mesh	Element Size	Number of Nodes	Number of Elements
#1	0.010	135755	318902
#2	0.009	161389	375538
#3	0.008	192169	449194
#4	0.006	328741	857145
#5	0.005	474400	1331034

Table 3.2: Solver parameters and boundary conditions for mesh independency study.

Solver	Pressure based – Steady state
Viscous model	Realizable k-e turbulence model Standard Wall Functions
Fluid material	Water Density, ρ = 998.2 kg/m3 Dynamic Viscosity, μ = 0.001003 kg/m-s)
Boundary condition	Velocity inlet at Nozzle = 8.2m/s (constant) Inlet Pressure at Nozzle = 6895000 Pa (constant) Outlet Pressure at the end Annulus = 0 Pa (constant) Inner and Outer wall of model = Stationary Wall and No Slip
Solution Methods	Pressure-Velocity coupling – Simple Discretization Scheme: Pressure – Standard Momentum – First order upwind Turbulent Kinetic Energy – First order upwind Specific Dissipation Rate – First order upwind

3.4 Preliminary Simulations

In ANSYS Fluent, the solver used is pressure-based with absolute velocity formulation running in steady state of time. Since this research only revolves around single phase flow, the multiphase model is turned off. Viscous model of realizable k-epsilon is selected with standard wall functions and default values for constants. In the parametric study, mud is inputted as a fluid under materials. Density of all muds are fixed to 1198 kg/m^3. Viscosity of the muds are governed Yield Power Law also known as Herschel-Bulkley model and it can be activated by inserting command lines into the Text User Interface (TUI) as shown in Figure 3.4. The use of Yield Power Law dependence on the availability of yield stress, τ_o in Table 3.4. Inlet velocity is varied according to flow rate over a fixed TFA as shown in Table 3.5. Once the solver parameters are settled as tabulated in Table 3.3, hybrid initialization method is initialized and followed by the run of calculation.

```
> define/

/define> models

/define/models> viscous

/define/models/viscous> turbulence-expert

/define/models/viscous/turbulence-expert> turb-non-newtonian
Enable turbulence for non-Newtonian fluids? [no] yes

/define/models/viscous/turbulence-expert>
```

Figure 3.4: Command lines to activate Yield Power Law model in ANSYS Fluent.

Table 3.3: Solver parameters and boundary conditions for preliminary simulations.

Solver	Pressure based – Steady state
Viscous model	Realizable k-e turbulence model Standard Wall Functions
Fluid material	Mud Density, ρ = 1198 kg/m3 Mud Dynamic Viscosity, μ = Yield Power Law/Herschel-Bulkley model (Refer to Table 3.4)
Boundary condition	Velocity inlet at Nozzle = Varying (Refer to Table 3.5) Inlet Pressure at Nozzle = 6895000 Pa (constant)

	Outlet Pressure at the end Annulus = 0 Pa (constant) Inner and Outer wall of model = Stationary Wall and No Slip
Solution Methods	Pressure-Velocity coupling – Simple Discretization Scheme: Pressure – Standard Momentum – First order upwind Turbulent Kinetic Energy – First order upwind Specific Dissipation Rate – First order upwind

Table 3.4: Mud Rheology for preliminary simulations.

Name/Type		Quality		Rheology			
		Details	**Weighting agent**	τ_o	k	n	$\dot{\gamma}_{crit}$
Water Based Mud [25]	WBM B	Bentonite	Barite	3.78	0.446	0.69	0.001
	WBM D	MMO-Bentonite	Barite	11.84	0.438	0.7	0.001

Table 3.5: Varying flow rate and inlet velocity over fixed TFA for preliminary simulations.

Flow Rate, Q (gpm)	Inlet Velocity, V_{in} (ft/s)
300	35.30
400	47.03
500	58.79
600	70.55
700	82.31
800	94.07

3.5 Parametric Study Simulations

Design of Experiments (DOE) is a technique used to scientifically determine the location of sampling points. There are a wide range of DOE algorithms or methods available in engineering literature. These techniques all have one common characteristic: they try to locate the sampling points such that the space of random input parameters is explored in the most efficient way, or obtain the required information with a minimum of sampling points. [34]

In the Latin Hypercube Sampling Design DOE type, the DOE is generated by the LHS algorithm, an advanced form of the Monte Carlo sampling method that avoids clustering samples. In a Latin Hypercube Sampling, the points are randomly generated in a square grid across the design space, but no two points share the same value. Possible disadvantages of an LHS design are that extremes (i.e., the corners of the design space) are not necessarily covered and that the selection of too few design points can result in a lower quality of response prediction. [34]

Central Composite Design (CCD) is the default DOE type. It provides a screening set to determine the overall trends of the meta-model to better guide the choice of options in Optimal Space-Filling Design. [34]

In the parametric study simulations, various muds rheology which are governed by yield power law are collected from past studies and compiled into upper and lower bounds in Table 3.6. These upper and lower bounds were inputted into ANSYS' Design of Experiments program. LHS design is chosen as it brings about no two points of equal value. CCD is used as backup when some of LHS' design points do not show expected results. Design points generated were compiled as shown in Table 3.8. Once the solver parameters are settled as tabulated in Table 3.7, hybrid initialization method is initialized and followed by the run of calculation.

Table 3.6: Upper and lower bound mud rheology variables govern by Yield Power Law for parametric study simulations.

Mud Rheology	Symbol	Unit	Min.	Max	Average
Volume Flow Rate	q	gpm	100	1000	550
Inlet Velocity	V_{in}	m/s	2.5	40	21.25
Yield Stress	τ_0	Pa	0.35	12	6.175
Consistency Index	K	Pa.s^n	0.031	9	4.5155
Power Low Exponent	n	-	0.2	0.9	0.55

Table 3.7: Solver parameters and boundary conditions for parametric study simulations.

Solver	Pressure based – Steady state
Viscous model	Realizable k-e turbulence model Standard Wall Functions
Fluid material	Mud Density, ρ = 1198 kg/m3 Mud Dynamic Viscosity, μ = Yield Power Law/Herschel-Bulkley model (Refer to Table 3.8)
Boundary condition	Velocity inlet at Nozzle = Varying (Refer to Table 3.8) Inlet Pressure at Nozzle = 6895000 Pa (constant) Outlet Pressure at the end Annulus = 0 Pa (constant) Inner and Outer wall of model = Stationary Wall and No Slip
Solution Methods	Pressure-Velocity coupling – Simple Discretization Scheme: Pressure – Standard Momentum – First order upwind Turbulent Kinetic Energy – First order upwind Specific Dissipation Rate – First order upwind

Table 3.8: Generated design points for parametric study simulations.

Design Points	V_{in} (ft/s)	τ_o (Pa)	K (Pa.s^n)	n	$\dot{\gamma}_{crit}$ (1/s)
#1	69.71785	4.9231	0.535	0.50086	0.001
#2	89.40289	8.0885	5.575	0.47722	0.001
#3	10.66273	5.8275	4.231	0.5245	0.001
#4	79.56037	10.8017	4.567	0.45358	0.001
#5	20.50525	2.2099	2.215	0.68998	0.001
#6	123.8517	7.1841	1.879	0.73726	0.001
#7	74.63911	8.5407	5.911	0.71362	0.001
#8	118.9304	3.1143	4.903	0.5245	0.001
#9	45.11155	8.9929	2.551	0.6427	0.001
#10	35.26903	2.6621	8.263	0.80818	0.001
#11	54.95407	5.8275	4.231	0.5245	0.001
#12	30.34777	10.3495	3.895	0.54814	0.001
#13	64.79659	9.8973	2.887	0.4063	0.001
#14	94.32415	4.4709	7.255	0.2881	0.001
#15	50.03281	11.2539	1.543	0.7609	0.001
#16	109.0879	5.8275	4.231	0.5245	0.001
#17	104.1667	3.5665	3.559	0.78454	0.001
#18	84.48163	6.2797	7.591	0.31174	0.001
#19	25.42651	5.8275	0.031	0.5245	0.001
#20	15.58399	7.6363	7.927	0.38266	0.001
#21	59.87533	6.7319	5.239	0.66634	0.001
#22	114.0092	9.4451	0.871	0.24082	0.001
#23	128.773	1.846976	1.273335	0.316407	0.001
#24	40.19029	1.7577	1.207	0.61906	0.001
#25	99.24541	0.4011	4.231	0.59542	0.001
#26	69.71785	9.808024	7.188665	0.316407	0.001
#27	89.40289	9.808024	7.188665	0.732593	0.001

3.6 Regression Analysis

After parametric study simulations over those 27 design points, pressure drop values are recorded in a CVS file and then imported back into ANSYS Design of Experiments under Custom Sampling Type. This is followed by the utilization of Response Surfaces.

The Response Surfaces are functions of different nature where the output parameters are described in terms of the input parameters. They are built from the Design of Experiments in order to provide quickly the approximated values of the output parameters, everywhere in the analyzed design space, without having to perform a complete solution. The accuracy of a response surface depends on several factors: complexity of the variations of the solution, number of points in the original Design of Experiments and choice of the response surface type. Several different meta-modeling algorithms are available to create the response surface. [34]

The default meta-modeling algorithm is Standard Response Surface - Full 2nd-Order Polynomial. Regression analysis is a statistical methodology that utilizes the relationship between two or more quantitative variables so that one dependent variable can be estimated from the others. A regression analysis assumes that there are a total of n sampling points and for each sampling point the corresponding values of the output parameters are known. Then the regression analysis determines the relationship between the input parameters and the output parameter based on these sample points. This relationship also depends on the chosen regression model. Typically for the regression model, a second-order polynomial is preferred. In general, this regression model is an approximation of the true input-to-output relationship and only in special cases does it yield a true and exact relationship. Once this relationship is determined, the resulting approximation of the output parameter as a function of the input variables is called the response surface. [34]

Kriging is a meta-modeling algorithm that provides an improved response quality and fits higher order variations of the output parameter. It is an accurate multidimensional interpolation combining a polynomial model similar to the one of the standard response surface—which provides a “global” model of the design space—plus local deviations so that the Kriging model interpolates the DOE points. The Kriging meta-model provides refinement capabilities for continuous input parameters, including

those with Manufacturable Values (not supported for discrete parameters). The effectiveness of the Kriging algorithm is based on the ability of its internal error estimator to improve response surface quality by generating refinement points and adding them to the areas of the response surface most in need of improvement. [34]

The Sparse Grid meta-model provides refinement capabilities for continuous parameters, including those with Manfacturable Values (not supported for discrete parameters). Sparse Grid uses an adaptive response surface, which means that it refines itself automatically. A dimension-adaptive algorithm allows it to determine which dimensions are most important to the objectives functions, thus reducing computational effort. [34]

Goodness of Fit shows information for any of the output parameters in a response surface. Goodness of Fit is closely related to the meta-model algorithm used to generate the response surface. [34]

Moreover, goodness of fit is affected by transformation type. There are 3 types of transformation available in ANSYS and they are Box-Cox, Yeo-Johnson, and None. By default, Yeo-Johnson transformation is used to compute the standard response surface regression because this transformation is more numerically stable in its back-transformation. On the other hand, Box-Cox transformation is numerically unstable but it provides better fit in certain case. And, None transformation simply means standard computation of response surface regression without any transformation.

3.7 Project Flow and Schedule

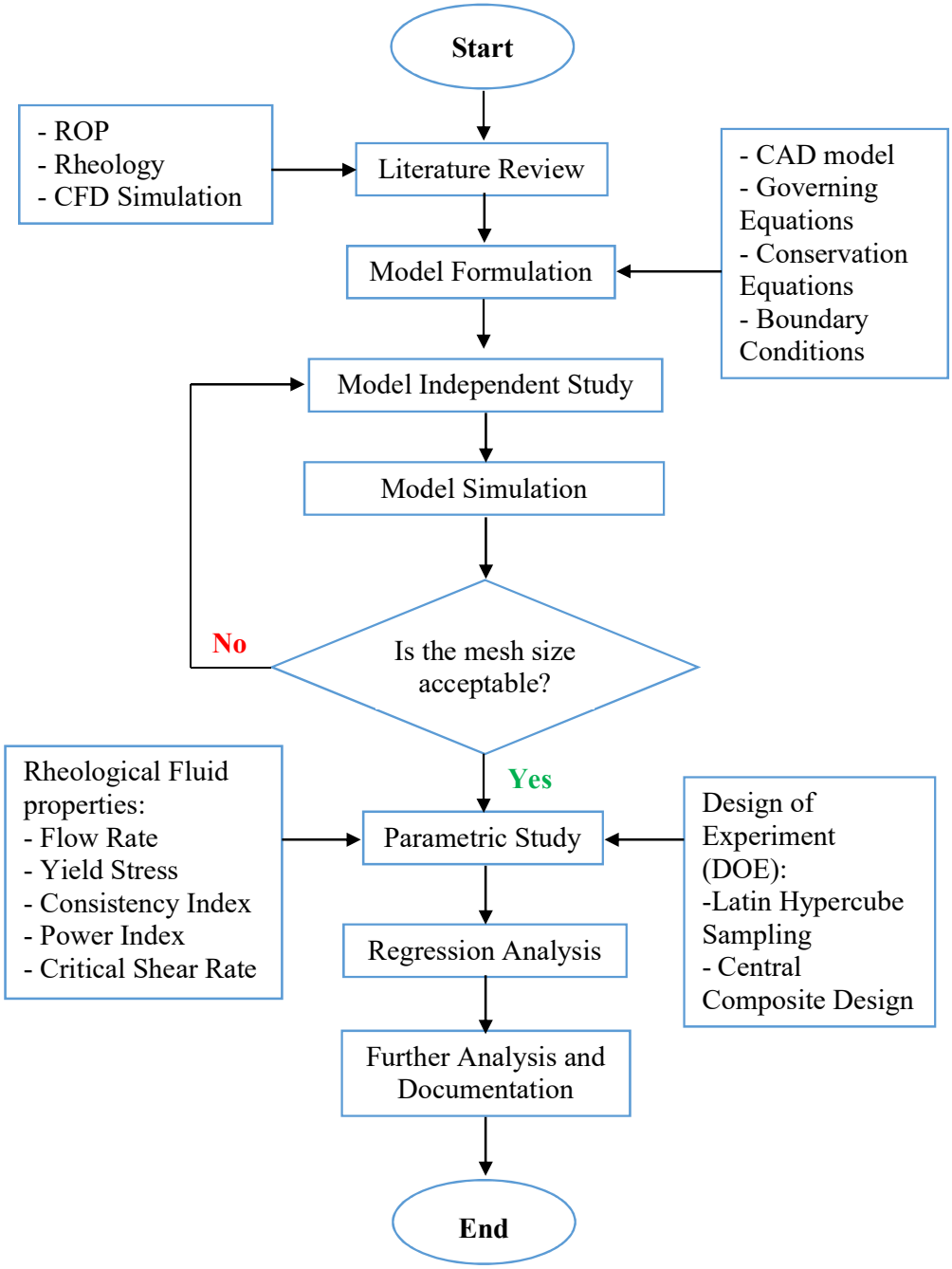

Figure 3.5: Project Flow Chart.

Activities	Weeks (FYP 1)													
	1	2	3	4	5	6	7	8	9	10	11	12	13	14
Literature Review														
Identifying Equation							m_1							
Geometry and Mesh Preparation														
Mesh Independency Simulations													m_2	
Preliminary Simulations														
Parametric Study Simulations														
Regression Analysis														
Further Result Analysis														
Report Writing														

Figure 3.6: Gantt chart of FYP1.

Activities	Weeks (FYP 2)													
	1	2	3	4	5	6	7	8	9	10	11	12	13	14
Literature Review														
Identifying Equation														
Geometry and Mesh Preparation														
Mesh Independency Simulations														
Preliminary Simulations														
Parametric Study Simulations														
Regression Analysis								m_3						
Further Result Analysis														
Report Writing													m_4	

Figure 3.7: Gantt chart of FYP2.

Table 3.9: Milestones throughout FYP 1 and 2.

No.	Milestone	Date
M_1	Identification of fundamental equation	7/11/2015
M_2	Simulation on various mesh size with little error percentage	12/12/2015
M_3	Simulation and modeling of research problem	30/01/2016
M_4	Further analysis of parametric study and final report completion	12/03/2016

Chapter 4: Results and Discussion

4.1 Mesh Independency Study

Computer Aided Design (CAD) of bottom hole annulus between the walls of formation and drill bit was imported into ANSYS Fluent and addressed with meshing of the model. Length of the model is 1.12m and diameter of 220mm. Figure 4.1 and Figure 4.2 shows the mesh generated on the CAD model.

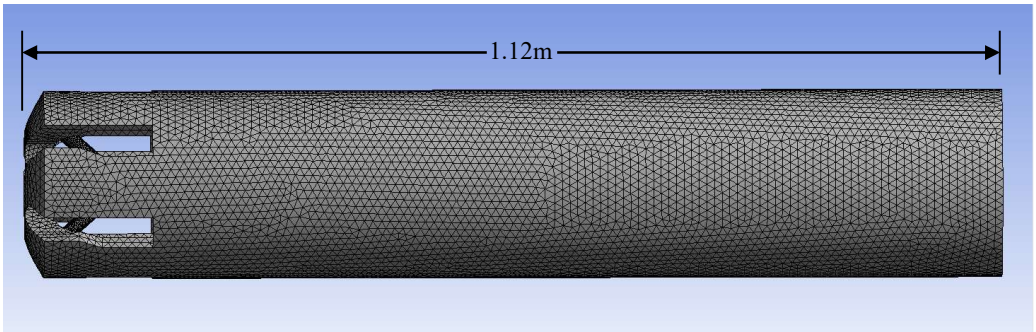

Figure 4.1: Side view of the meshed CAD model.

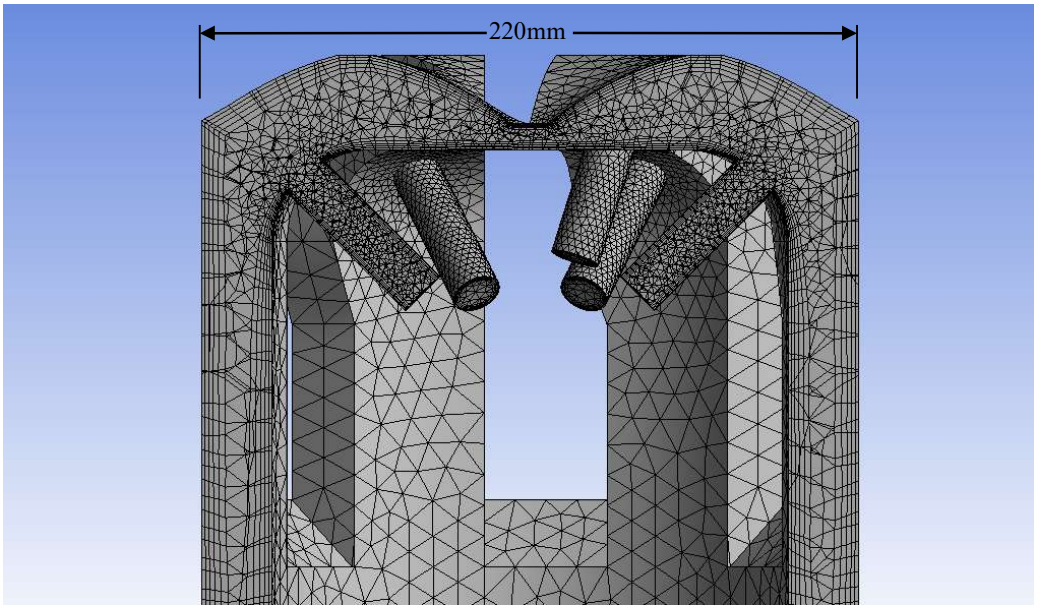

Figure 4.2: Cross-sectioned view of the meshed CAD model.

CFD simulations with steady state condition and single phase fluid were carried out for six cases by varying the element sizes to analyze mesh sensitivity. No rotation on the drill bit was considered. Table 4.1 shows the grid size and the computational time for each mesh while Table 4.2 shows the convergence data recorded.

Table 4.1: Grid size and computation time.

Mesh	Element Size	Number of Nodes	Number of Elements	Time Taken (HH:MM)
#1	0.010	135755	318902	00:10
#2	0.009	161389	375538	00:15
#3	0.008	192169	449194	00:23
#4	0.006	328741	857145	01:00
#5	0.005	474400	1331034	01:45

Table 4.2: Convergence data for each mesh.

Mesh	Iterations	continuity	x-velocity	y-velocity	z-velocity	k	epsilon	Average Pressure (Pa)	Average Velocity (ft/s)
#1	324	9.99 E-04	3.49 E-06	9.73 E-06	5.07 E-06	9.07 E-06	1.24 E-05	1.5206	0.02611
#2	253	9.90 E-04	6.45 E-06	2.16 E-05	5.72 E-06	1.53 E-05	3.94 E-05	1.5195	0.02611
#3	371	9.99 E-04	4.60 E-06	1.15 E-05	5.86 E-06	1.58 E-05	3.89 E-05	1.5202	0.02611
#4	489	9.97 E-04	3.84 E-06	1.17 E-05	5.55 E-06	7.65 E-06	1.67 E-05	1.4956	0.02611
#5	754	9.99 E-04	5.46 E-06	9.81 E-06	6.53 E-06	9.22 E-06	2.42 E-05	1.4959	0.02611

4.1.1 Comparative Study on Various Mesh Sizes

Based on data tabulated in Table 4.2, graphs of static pressure and velocity magnitude against element size of mesh were plotted below in as shown in Figure 4.3 to 4.6.

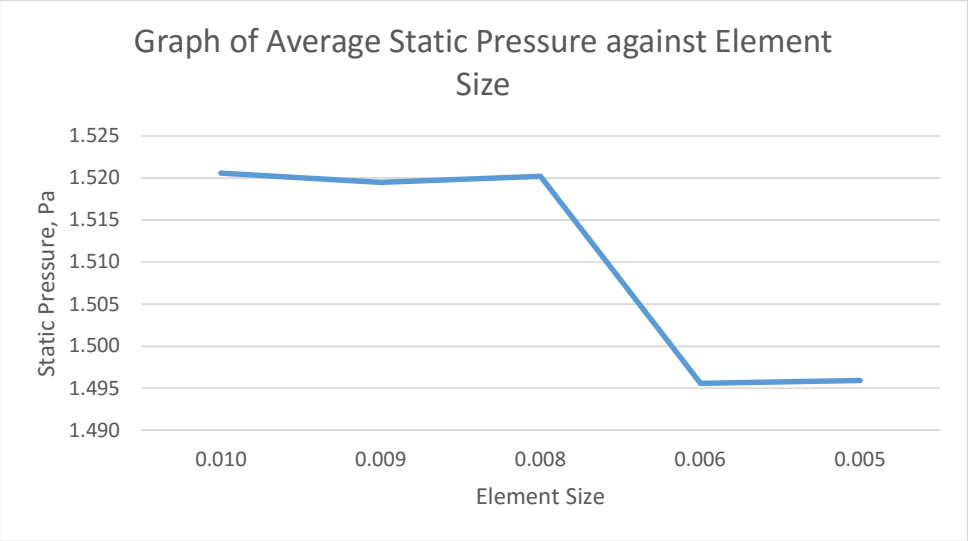

Figure 4.3: Graph of Average Static Pressure against Element Size.

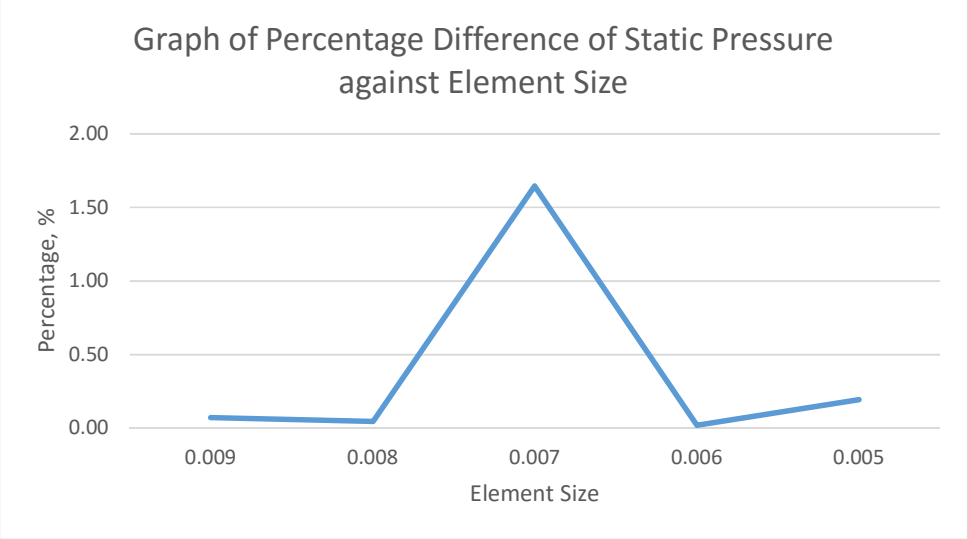

Figure 4.4: Graph of Percentage Difference of Static Pressure against Element Size.

Static Pressure: The static pressure appears to decrease as element size gets finer. The percentage difference between element size of 0.006 and 0.005 is 0.02%. These 2 element sizes are within the targeted less than 5% of mesh independence study.

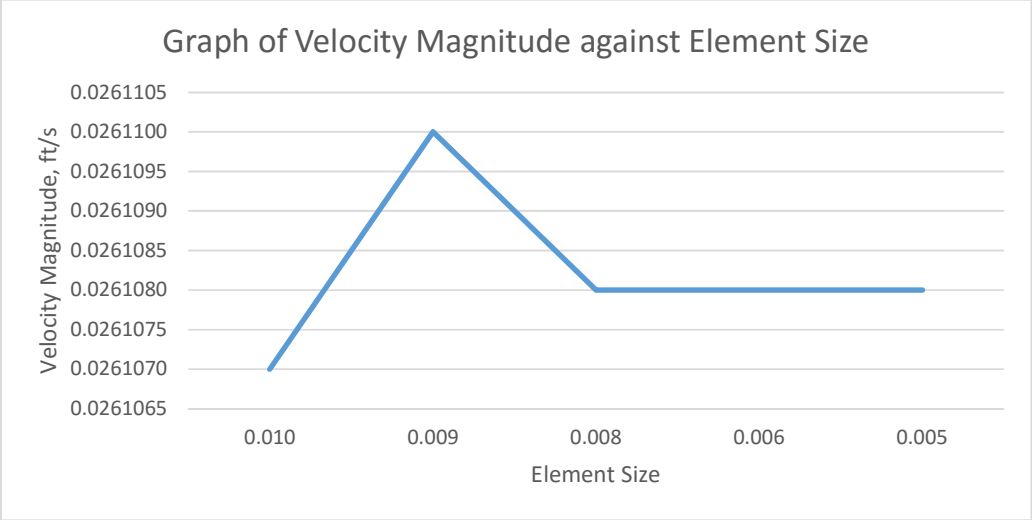

Figure 4.5: Graph of Average Velocity Magnitude against Element Size.

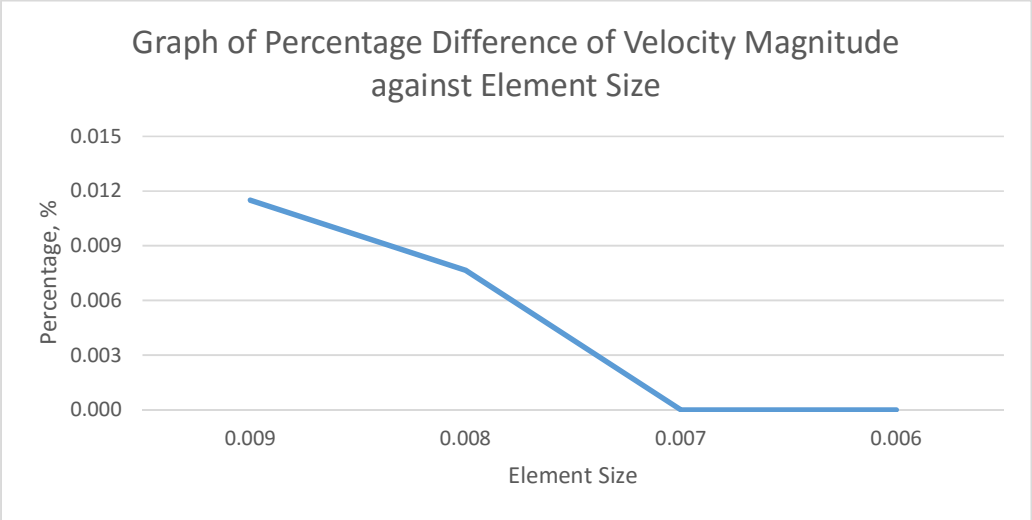

Figure 4.6: Graph of Percentage Difference of Velocity Magnitude against Element Size.

Velocity Magnitude: As element size gets finer, the average velocity magnitude shows consistency of 0.0261020ft/s from element size of 0.008 to 0.005. The percentage difference between element size of 0.008, 0.006, and 0.005 is 0.0%. These 3 element sizes are within the targeted less than 5% of mesh independence study.

Comparison Summary: The finer and smaller the element size of mesh, the higher the accuracy of the simulation. Potential element sizes from graphs of static pressure and velocity magnitude vs. element sizes are 0.006 and 0.005. These 2 sizes are of very small percentage difference amongst themselves. Given that the time taken to simulate with each mesh sizes in Table 4.1, element size of 0.006 appears to be the best candidate for optimized mesh resolution. It is capable of accurate results, on par with finer element size of 0.005, and the time taken for simulation is about 42% faster than neighboring element size of 0.005. Henceforth, Element size of 0.006 is used for future simulations.

4.2 Preliminary Simulations

Based on mesh independence study, mesh size of 0.06 provides consistent results within optimal time. Hence, further simulations are conducted using this particular mesh size. WBM B and D are governed by Yield Power Law from Table 3.4 and these muds were used for the preliminary simulations. Flow rate of muds ranged from 300 to 800 gpm. Inlet velocities were calculated over the fixed TFA of CAD PDC bit model. Inlet velocities of the muds are tabulated in Table 3.5. Inlet pressures were recorded while values for outlet pressures were offset away from outlet boundary. This is because direct collection of data from the outlet boundary may give inaccurate data. Pressure drop across bit results from preliminary simulation is tabulated in Table 4.3 and plotted in Figure 4.7.

Table 4.3: Pressure drop across bit results from preliminary simulation.

Flow Rate, Q (gpm)		300	400	500	600	700	800
WBM B	Inlet Pressure, P_{in} (Pa)	155,717	186,048	217,693	256,031	294,974	343,537
	Outlet Pressure, P_{out} (Pa)	103,151	103,760	104,399	105,224	105,610	106,372
	Pressure Drop, ΔP (Pa)	52,566	82,288	113293	150807	189364	237164
WBM D	Inlet Pressure, P_{in} (Pa)	176,200	209,900	247,800	289,700	335,200	385,400
	Outlet Pressure, P_{out} (Pa)	104,000	104,900	105,700	106,600	107,500	108,500
	Pressure Drop, ΔP (Pa)	72200	105000	142100	183100	227700	276900

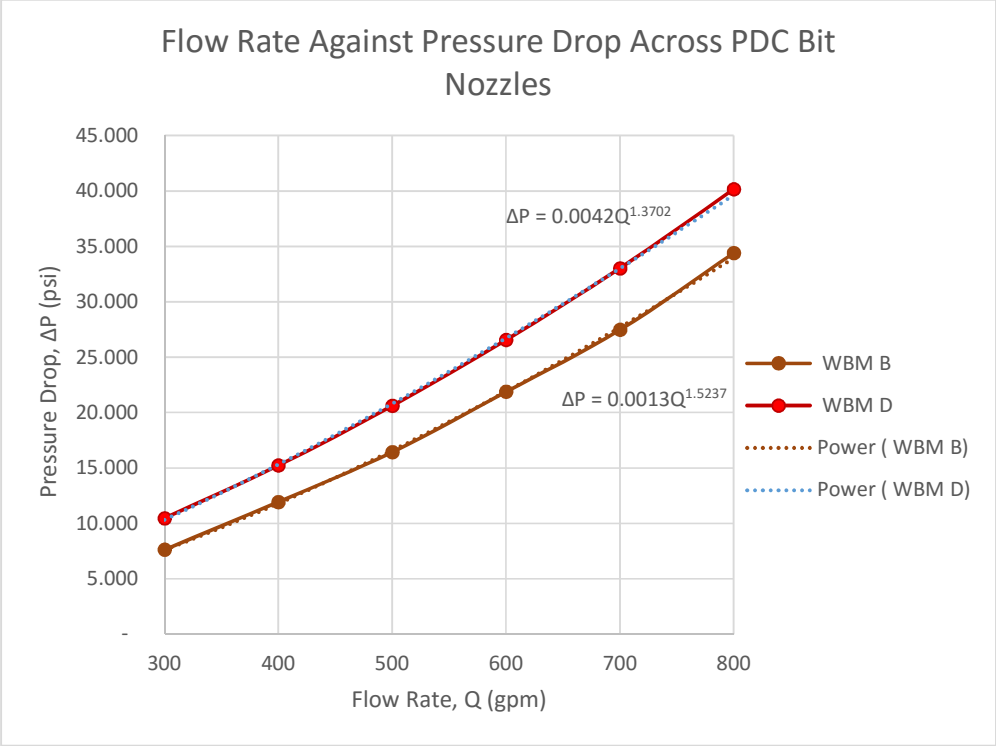

Figure 4.7: Graph of Flow Rate Against Pressure Drop Across PDC Bit Nozzles for WBM B and D.

4.2.1 Comparative Study on Various Pressure Models

Many previous studies had been done on pressure drop models across bit. However, none of the existing models are in terms of mud rheology. For comparison, the pressure drop across bit models have been compiled in Table 4.4. And, under the same range of flow rate, fixed TFA, and fixed mud weight, theoretical calculations were done and tabulated in Table 4.5 and visual comparison in Figure 4.8.

Table 4.4: Previous study on pressure drop across bit.

Source	Equations	Description
Monicard [35]	$\Delta P_b = \frac{(MW)(Q^2)}{11884(C_d{}^2)(TFA^2)}$	C_d = 0.8 (Conventional Bit) C_d = 0.95 (Jet Bit)
Ramsey, Warren, and Robinson. [18, 36, 37]	$\Delta P_b = \frac{(MW)(Q^2)}{12032(C_d{}^2)(TFA^2)}$	C_d = 1.03
Lyons [19]	$\Delta P_b = \frac{(MW)(Q^2)}{8795[(TFA)(e^{-0.832})(\frac{ROP}{RPM})]^2}$	ROP and RPM

Table 4.5: Calculated results of previous study compiled with preliminary simulation on pressure drop across bit with fixed TFA over varying flow rate.

Flow Rate	Q (gpm)	300	400	500	600	700	800
Monicard, C_d=0.8	ΔP_b (kPa)	109.7	194.9	304.5	438.5	596.9	779.6
Monicard, C_d=0.95		77.7	138.2	216.0	311.0	423.3	552.8
Ramsey, Warren, and Robinson, C_d=1.03		65.3	116.1	181.5	261.3	355.6	464.5
Lyons, ROP and RPM		68.7	122.1	190.8	274.7	373.9	488.3
WBM B		52.6	82.3	113.3	150.8	189.4	237.2
WBM D		72.2	105.0	142.1	183.1	227.7	276.9

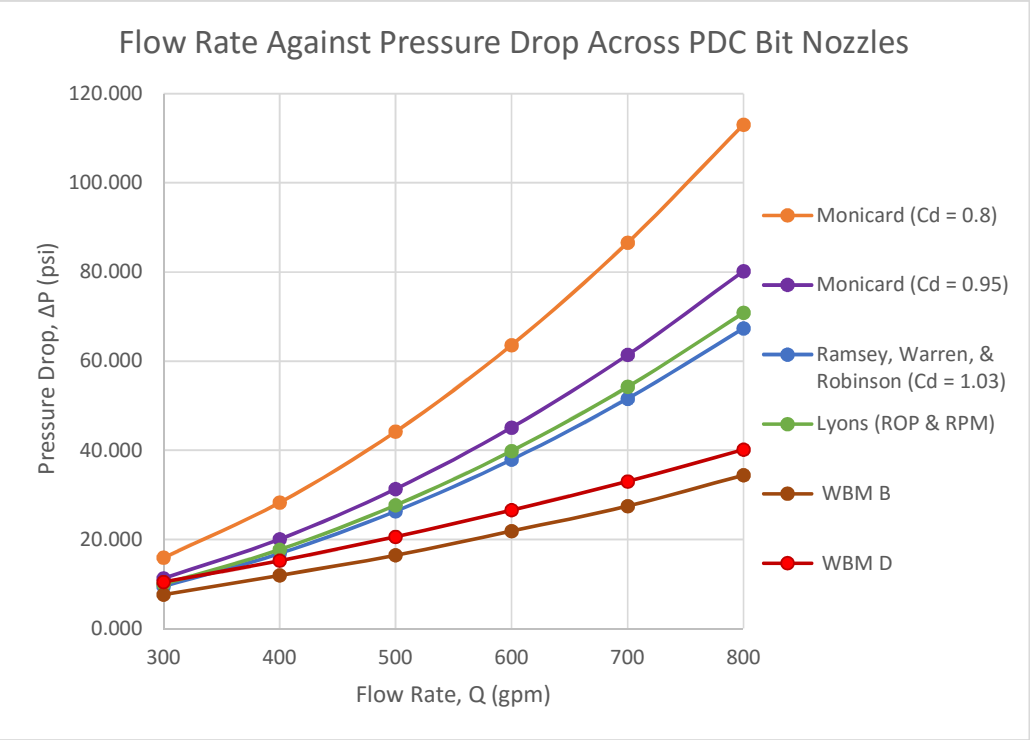

Figure 4.8: Graph of Flow Rate Against Pressure Drop Across PDC Bit Nozzles for WBM B and D.

Comparison Summary: When mud flow rate increases, the pressure drop across bit increases. However, both simulations on WBMs rheology show smaller pressure drop across bit nozzles as flow rate increases. The smaller the shear stress (τ) of WBM, the smaller the drop in pressure. Rheological properties have significant positive effect on pressure drop; up to 50% reduction in losses.

4.3 Parametric Study and Regression Analysis

Type of DOE used to generate design points are mainly by Latin Hypercube Sampling with a few by Central Composite Design. This is because some of design points from LHS did not simulate expected result where the pressure drop is too small which means invalid result. To overcome this problem, CCD was used to sample additional design points and simulated results substituted those invalid results. Inlet pressures were recorded while values for outlet pressures were offset away from outlet boundary. This is because direct collection of data from the outlet boundary may give inaccurate data as shown in Figure 4.9.

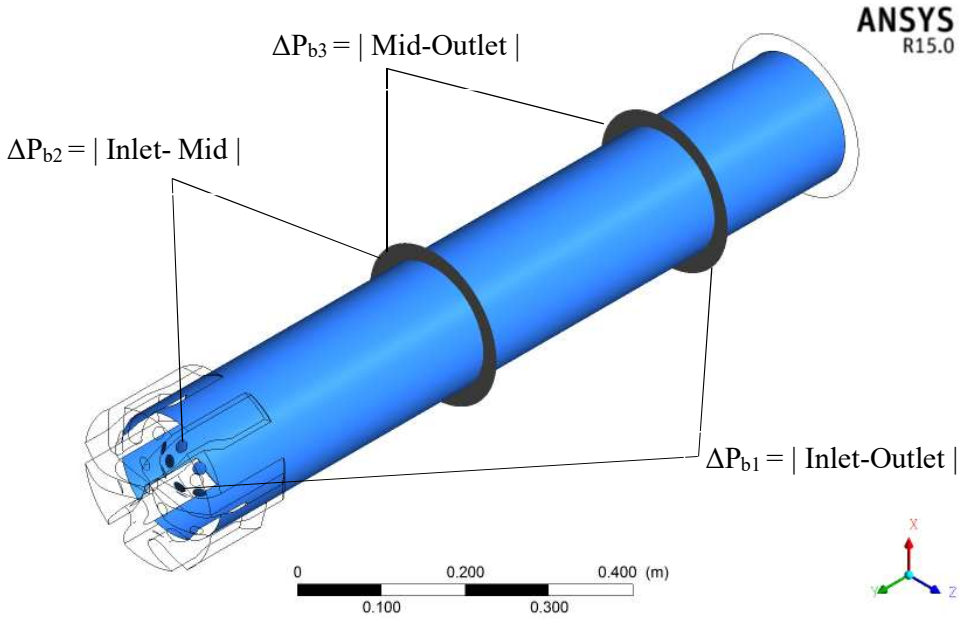

Figure 4.9: Pressure drop data points for this project. The outlet plane is offset away from the outlet to avoid boundary conditions and to obtain more accurate data.

4.3.1 Results on Parametric Study

Based on Table 3.6, a total of 27 design points were generated using LHS and CCD. Simulation parameters were inputted accordingly. Simulations were run and the data are tabulated in Table 4.6. Visual plots are shown in Figure 4.10 to 4.12.

Table 4.6: Tabulated pressure drop across bit results from parametric study simulations.

Design Points	V_{in} (m/s)	τ_o (Pa)	K (Pa.s^n)	n	ΔP_{b1} Inlet-Outlet (Pa)	ΔP_{b2} Inlet-Mid (Pa)	ΔP_{b3} Mid-Outlet (Pa)
#1	21.25	4.9231	0.535	0.50086	70480.6	69113.8	1366.84
#2	27.25	8.0885	5.575	0.47722	117731	116089	1641.77
#3	21.25	5.8275	4.231	0.5245	76312.1	73306.8	3005.33
#4	24.25	10.8017	4.567	0.45358	93929.3	92850.3	1078.92
#5	6.25	2.2099	2.215	0.68998	10994	10293.9	700.094
#6	37.75	7.1841	1.879	0.73726	266571	259852	6718.42
#7	22.75	8.5407	5.911	0.71362	122201	115894	6307.25
#8	36.25	3.1143	4.903	0.5245	206823	204741	2081.3
#9	13.75	8.9929	2.551	0.6427	36740	35583.7	1156.27
#10	10.75	2.6621	8.263	0.80818	125681	116077	9604.47
#11	2.5	5.8275	4.231	0.5245	1921.45	1586.65	334.797
#12	9.25	10.3495	3.895	0.54814	16774.1	16071.4	702.688
#13	19.75	9.8973	2.887	0.4063	62770.1	61674.9	1095.19
#14	28.75	4.4709	7.255	0.2881	131796	122750	9045.91
#15	15.25	11.2539	1.543	0.7609	54838.3	52053.9	2784.32
#16	40	5.8275	4.231	0.5245	248054	247052	1002.48
#17	31.75	3.5665	3.559	0.78454	276562	264131	12430.8
#18	25.75	6.2797	7.591	0.31174	111314	100513	10800.4
#19	21.25	5.8275	0.031	0.5245	69779.5	68429	1350.56
#20	4.75	7.6363	7.927	0.38266	4793.55	4420.16	373.391
#21	18.25	6.7319	5.239	0.66634	68640.6	65826.7	2813.95
#22	34.75	9.4451	0.871	0.24082	182346	181169	1177.11
#23	8.046	1.84698	1.27334	0.31641	10350.5	10243.9	106.531
#24	12.25	1.7577	1.207	0.61906	26038.1	25527.2	510.836
#25	30.25	0.4011	4.231	0.59542	152310	150681	1628.41
#26	8.046	9.80802	7.18867	0.31641	11910.3	11465.3	445.039
#27	34.45	9.80802	7.18867	0.73260	279103	265759	13344.2

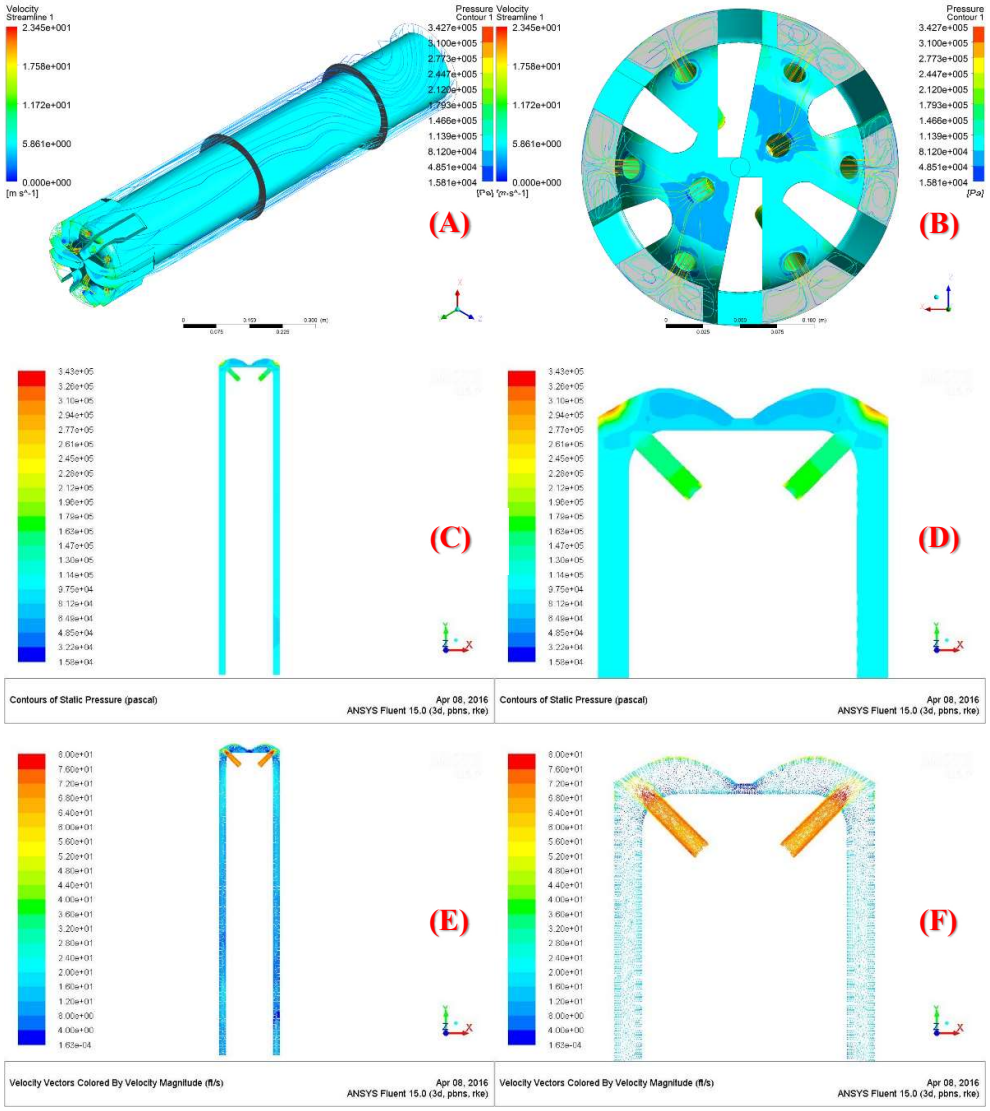

Figure 4.10: Visual plots for overall average input parameters. (A) Isometric view with velocity vertor and presure countour. (B) Bit Face view with velocity vertor and presure countour. (C) Presure countour of X-Y crosss-section of the model. (D) Presure countour of X-Y crosss-section of the nozzles. (E) Velocity vector of X-Y crosss-section of the model. (F) Velocity vector of X-Y crosss-section of the nozzles.

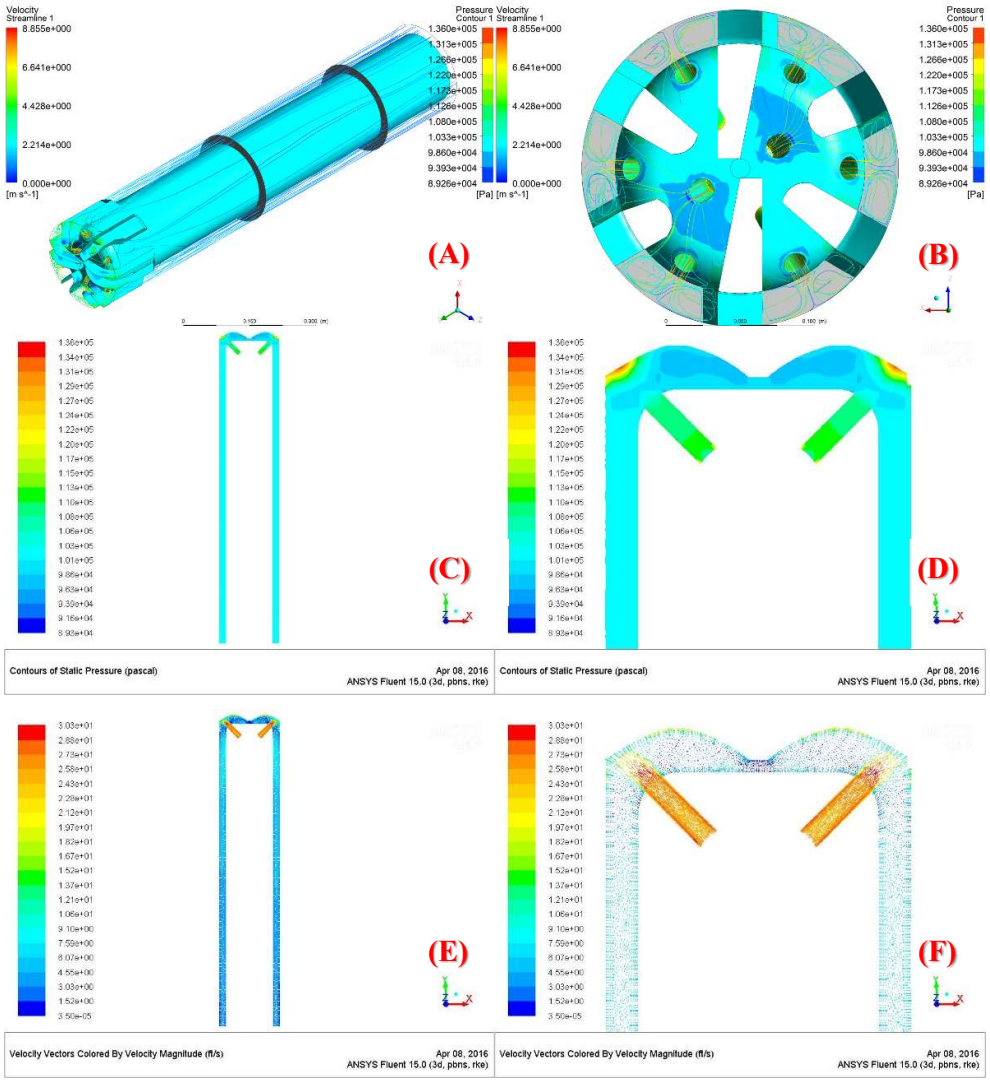

Figure 4.11: Visual plots for overall minimum input parameters. (A) Isometric view with velocity vertor and presure countour. (B) Bit Face view with velocity vertor and presure countour. (C) Presure countour of X-Y crosss-section of the model. (D) Presure countour of X-Y crosss-section of the nozzles. (E) Velocity vector of X-Y crosss-section of the model. (F) Velocity vector of X-Y crosss-section of the nozzles.

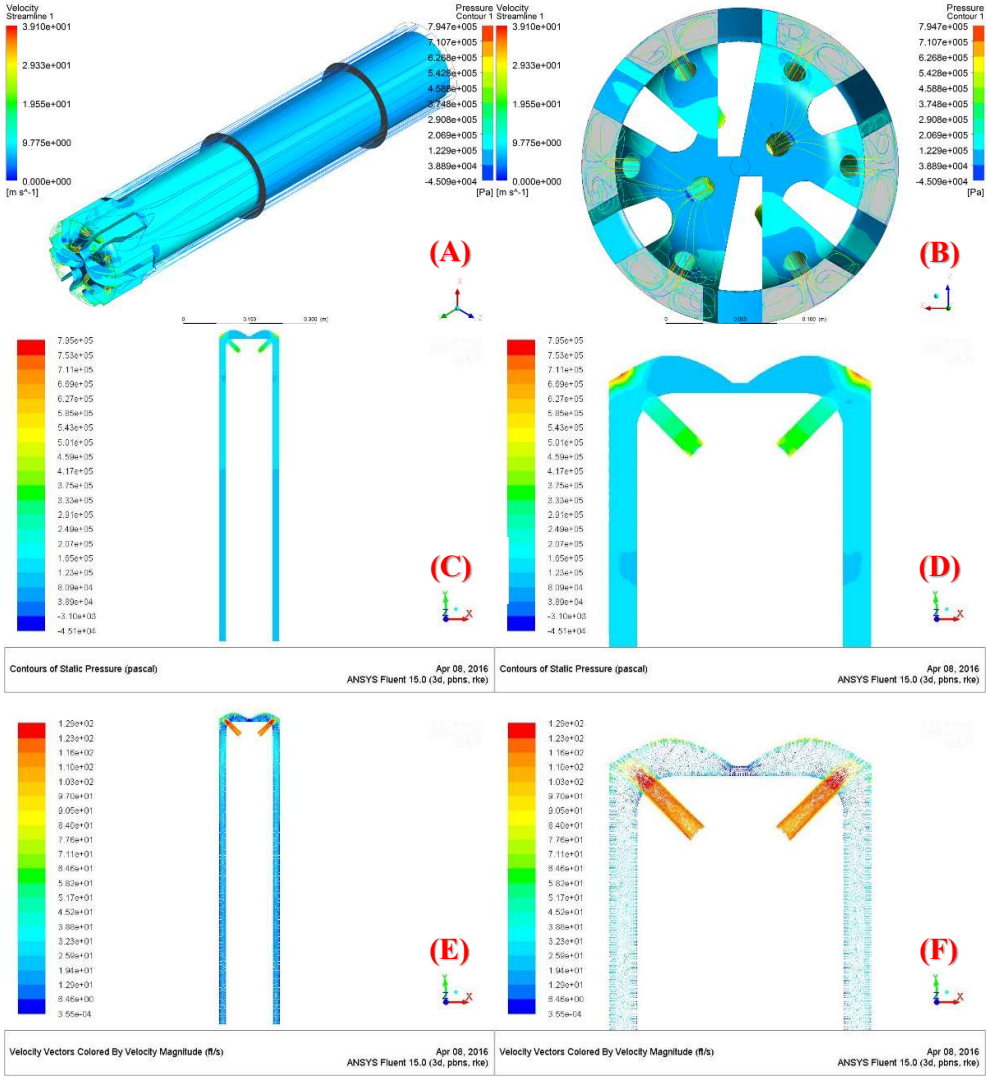

Figure 4.12: Visual plots for overall maximum input parameters. (A) Isometric view with velocity vertor and presure countour. (B) Bit Face view with velocity vertor and presure countour. (C) Presure countour of X-Y crosss-section of the model. (D) Presure countour of X-Y crosss-section of the nozzles. (E) Velocity vector of X-Y crosss-section of the model. (F) Velocity vector of X-Y crosss-section of the nozzles.

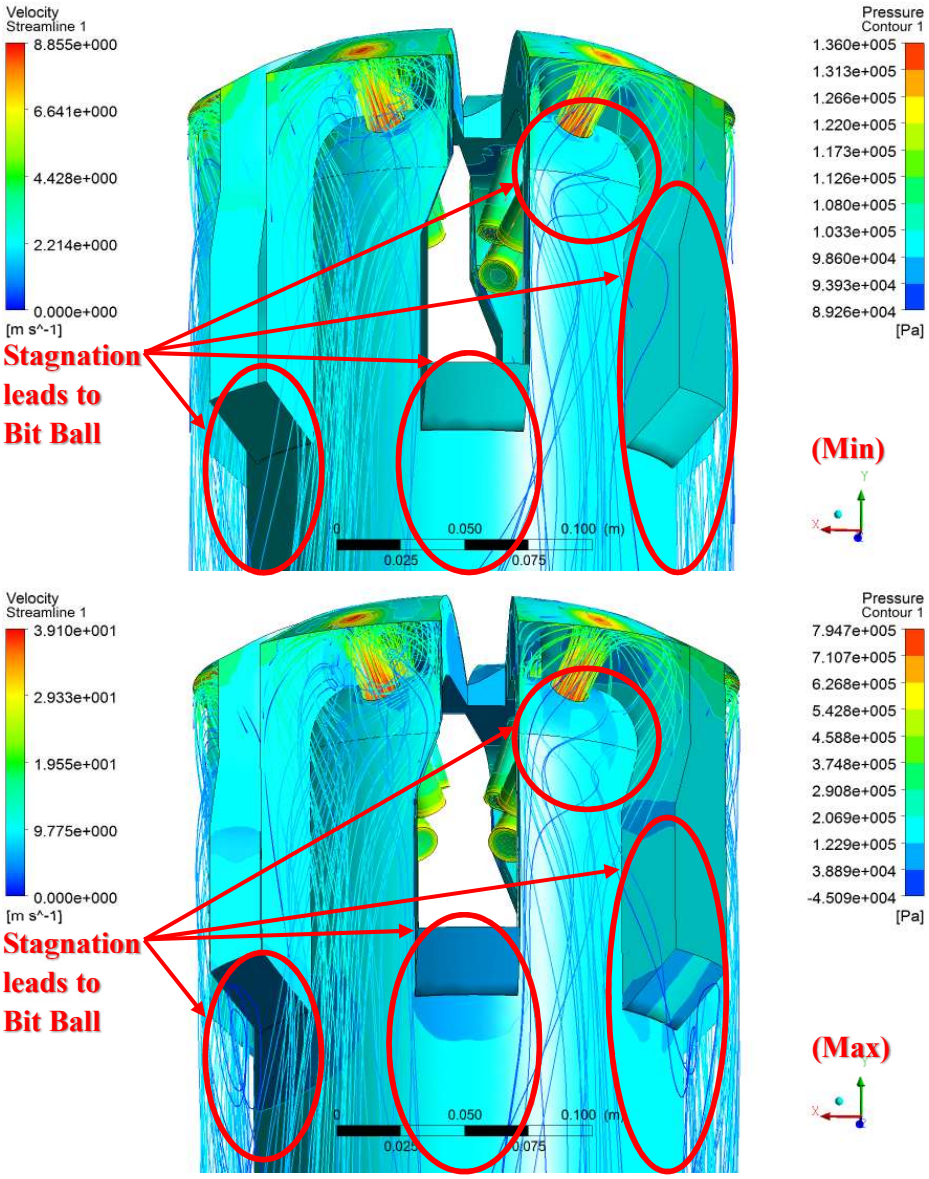

Figure 4.13: Top and bottom represents overall input parameters at mininum and maximum each respectively.

Stagnation points are indications of bit balling as shown in Figure 4.13. These points have very little or no velocity vector paths which means mud would be not circulated at these points. No proper mud circulation would definitely lead to bit ball despite high or low input parameters (emphasis on flow velocity). This can be concluded with bad geometry of the model and an optimized tweak to the geometry would eliminate the probability of bit balling.

4.3.2 Comparative Study on Regression Models

There are a total of 4 types of Response Surfaces which are Standard Response Surface, Kriging, Non-Parametric Regression, and Neural Network. Goodness of Fit for each type of response surfaces are plotted as shown in Figure 4.14 to 4.17 and quantitative details are tabulated in Table 4.7. Based on Figure 4.15, the design points in all Goodness of Fit graphs are generally inline linearly. The red and Green dots, which represents $\Delta P_{b1\ (Inlet\text{-}Outlet)}$ and $\Delta P_{b2\ (Inlet\text{-}Mid)}$ respectively, are noticebly inline linealy and consistenly over all 4 types of response surfaces. However, the blue dots, which represents $\Delta P_{b3\ (Mid\text{-}Outlet)}$, tend to be disoriented and dispersed in the Neutral Network. And, they appear to be closer to the linear line with Standard Response Surface Visually, Kriging and Non-Parametric Regression Response Surfaces would give the best Goodness of Fit.

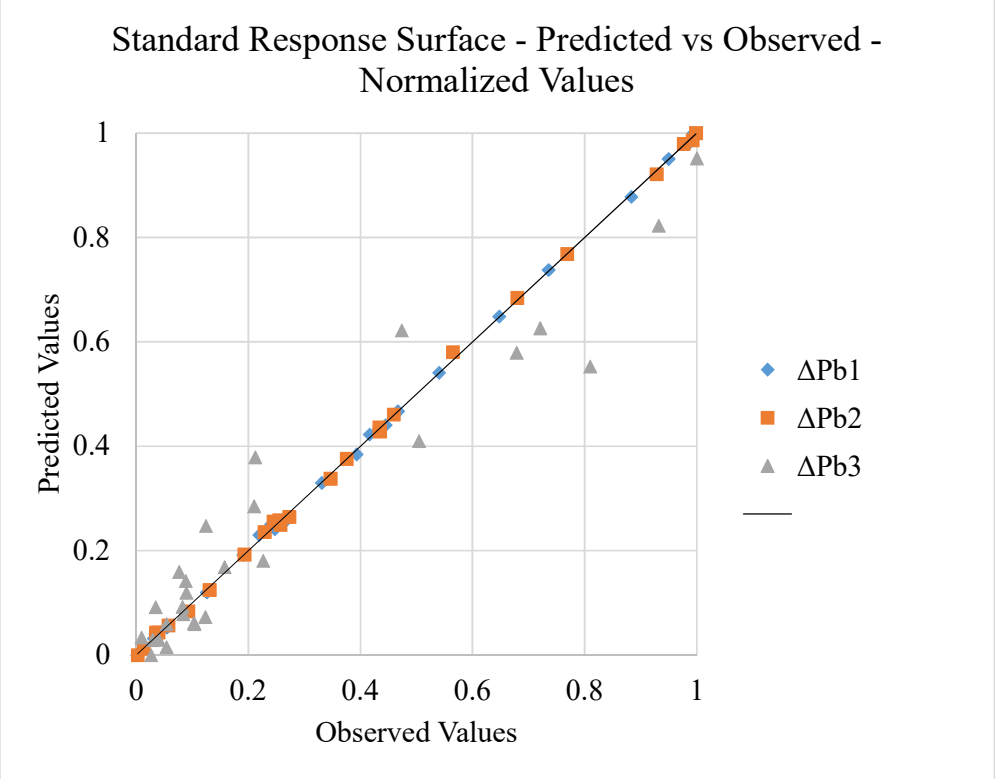

Figure 4.14: Goodness of Fit generated over Standard Response Surface.

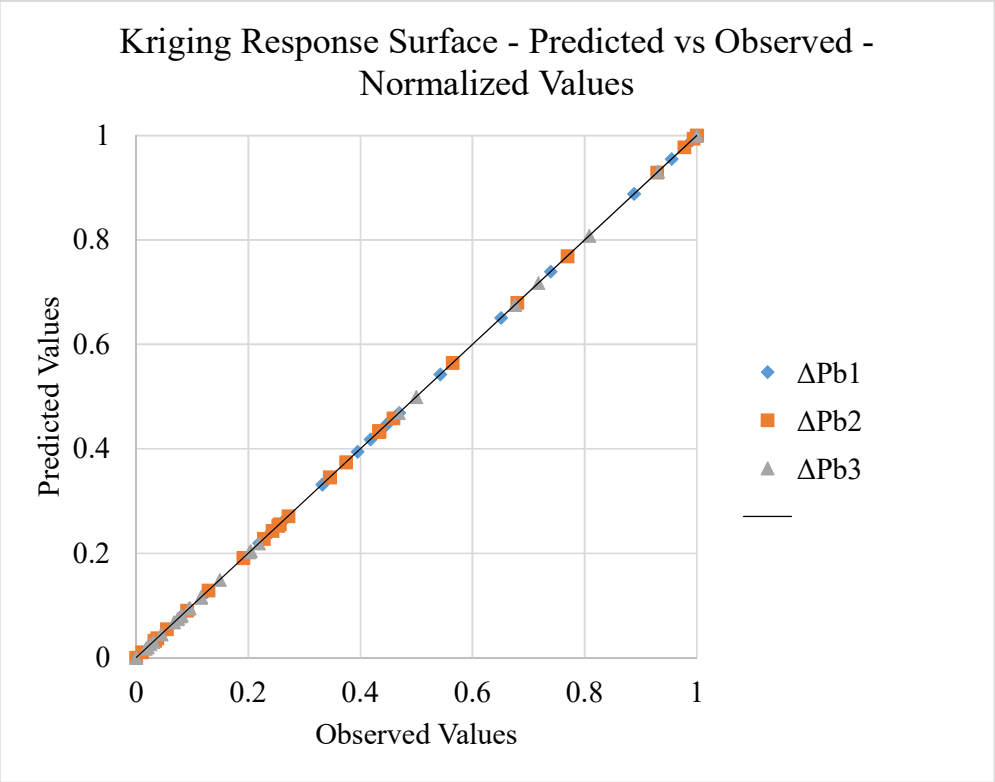

Figure 4.15: Goodness of Fit generated over Kriging Response Surface.

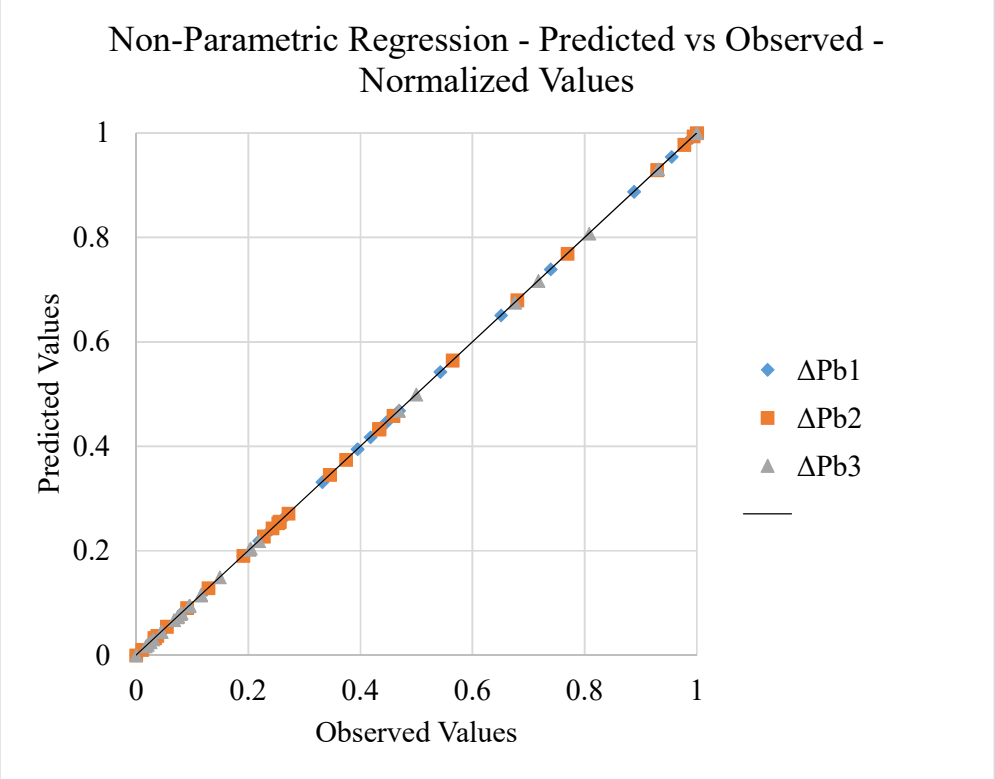

Figure 4.16: Goodness of Fit generated over Non-Parametric Regression.

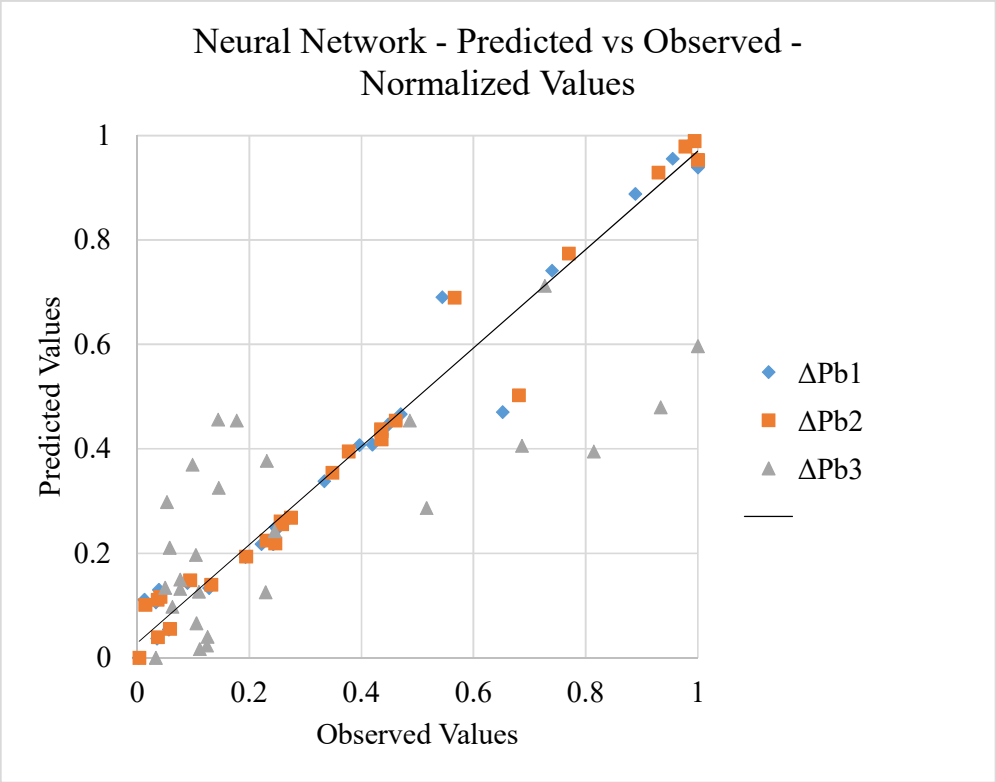

Figure 4.17: Goodness of Fit generated over Neural Network.

Table 4.7: Goodness of Fit details on various types of Response Surfaces.

Standard Response Surface	***ΔPb1***	***ΔPb2***	***ΔPb3***
Coefficient of Determination (Best Value = 1)	0.999703	0.999613	0.915067
Adjusted Coeff. of Determination (Best Value = 1)	0.999449	0.999329	0.87732
Maximum Relative Residual (Best Value = 0%)	20.39681	42.97441	303.4657
Root Mean Square Error (Best Value = 0)	1487.961	1651.019	1162.45
Relative Root Mean Square Error (Best Value = 0%)	5.927924	9.906101	82.2511
Relative Maximum Absolute Error (Best Value = 0%)	3.427116	4.86304	84.51619
Relative Average Absolute Error (Best Value = 0%)	1.335262	1.540253	21.38118
Kriging	***ΔPb1***	***ΔPb2***	***ΔPb3***
Coefficient of Determination (Best Value = 1)	1	1	1
Adjusted Coeff. of Determination (Best Value = 1)	0	0	0
Maximum Relative Residual (Best Value = 0%)	**0.000336**	**0.000302**	**5.73E-05**
Root Mean Square Error (Best Value = 0)	0	0	0
Relative Root Mean Square Error (Best Value = 0%)	0	0	0
Relative Maximum Absolute Error (Best Value = 0%)	0	0	0
Relative Average Absolute Error (Best Value = 0%)	1	1	1

Non-Parametric Regression	ΔP_{b1}	ΔP_{b2}	ΔP_{b3}
Coefficient of Determination (Best Value = 1)	1	1	1
Adjusted Coeff. of Determination (Best Value = 1)	0	0	0
Maximum Relative Residual (Best Value = 0%)	0.000879	0.001188	4.92E-05
Root Mean Square Error (Best Value = 0)	0	0	0
Relative Root Mean Square Error (Best Value = 0%)	0	0	0
Relative Maximum Absolute Error (Best Value = 0%)	0	0	0
Relative Average Absolute Error (Best Value = 0%)	1	1	1
Neural Network	ΔP_{b1}	ΔP_{b2}	ΔP_{b3}
Coefficient of Determination (Best Value = 1)	0.967238	0.973092	0.508332
Adjusted Coeff. of Determination (Best Value = 1)	569.5013	519.4872	900.0638
Maximum Relative Residual (Best Value = 0%)	15630.73	13763.88	2796.876
Root Mean Square Error (Best Value = 0)	123.9189	113.338	250.962
Relative Root Mean Square Error (Best Value = 0%)	57.23	55.28706	152.7558
Relative Maximum Absolute Error (Best Value = 0%)	9.255837	8.831413	52.80759
Relative Average Absolute Error (Best Value = 0%)	0.967238	0.973092	0.508332

Quantitatively, Kriging and Non-Parametric Regression Response Surface types shows good readings. These 2 types of response surfaces generate a good response charts. Since, Kriging and Non-Parametric Regression Response Surface types show good results in Goodness of Fit, it is wise to use either one for the generation of Response Chart. Given that both of these Response Surface Types are very much similar, Kriging is chosen because its data in Table 4.7 shows lower Maximum Relative Residual percentage.

4.3.3 Response Charts

All response charts are plotted in terms of XYZ axes which V_{in}, $\Delta P_{b,}$ and either τ_o, K, or n each respectively. This is done as such to study the correlation between the parameters. 2D charts are plotted in Figure 4.18 to 4.21. And 3D charts are plotted in Figure 4.22 to 4.30.

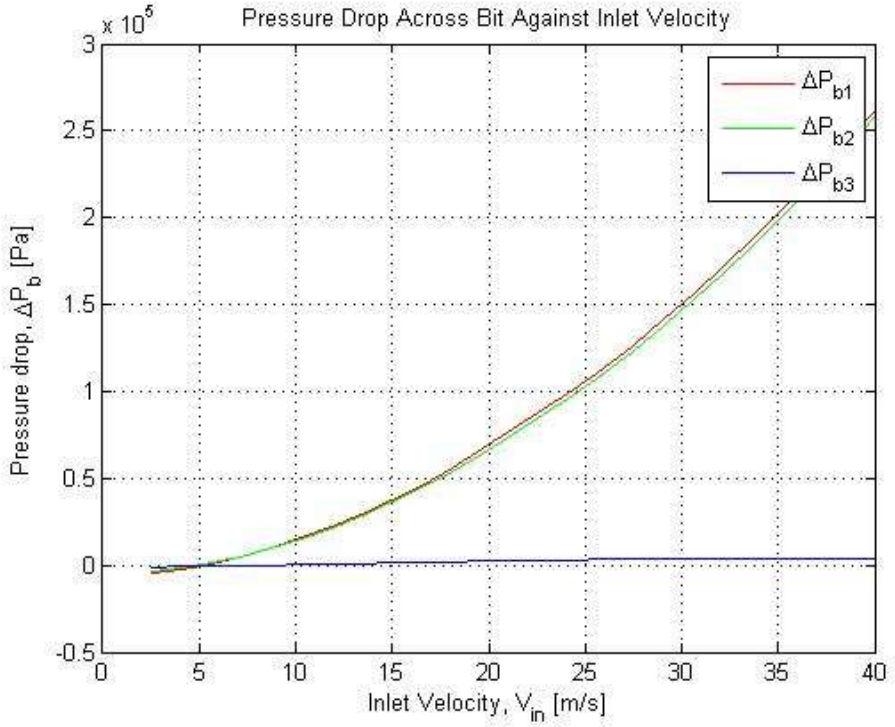

Figure 4.18: 2D Response Charts of ΔP_b against V_{in}.

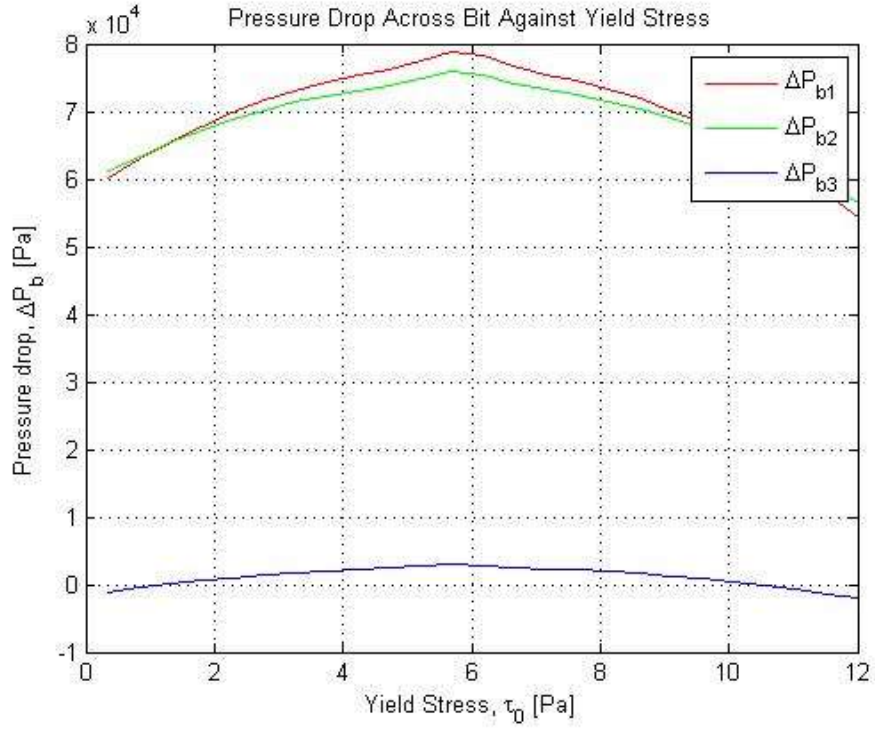

Figure 4.19: 2D Response Charts ΔP_b of against τ_o.

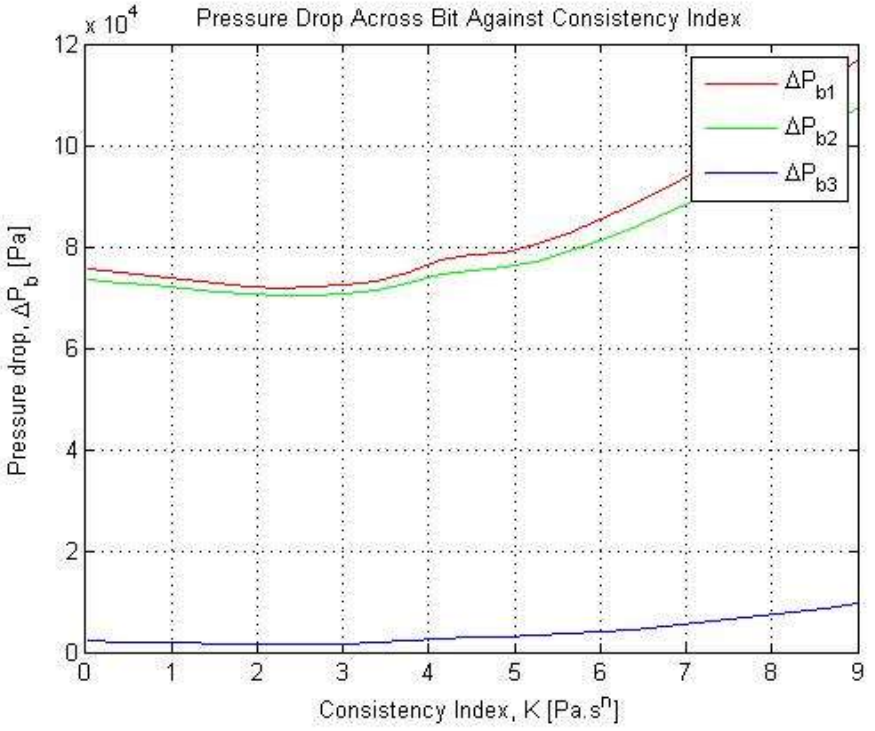

Figure 4.20: 2D Response Charts of ΔP_b against K.

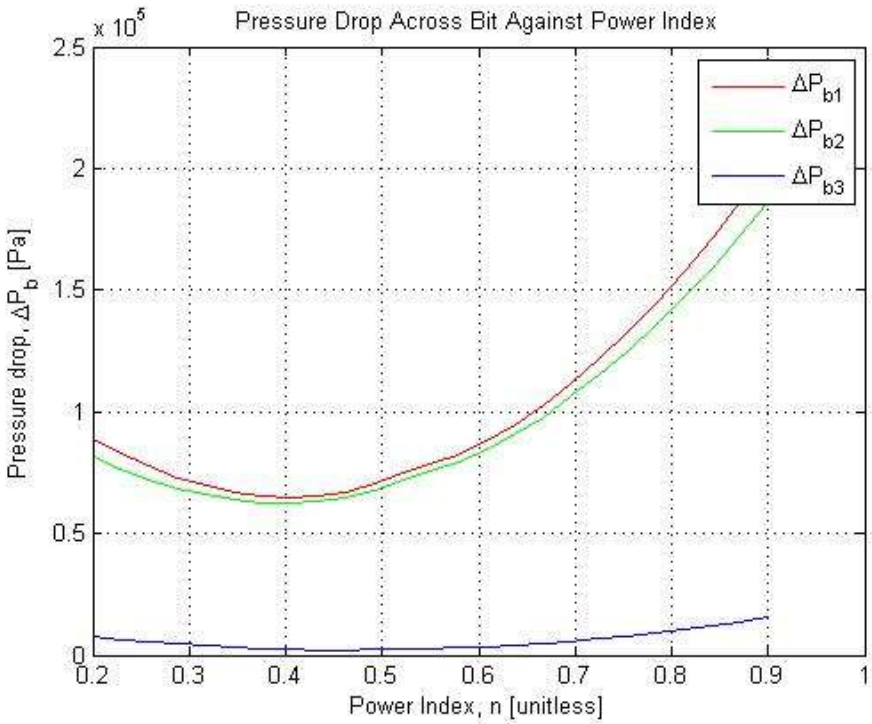

Figure 4.21: 2D Response Charts of ΔP_b against n.

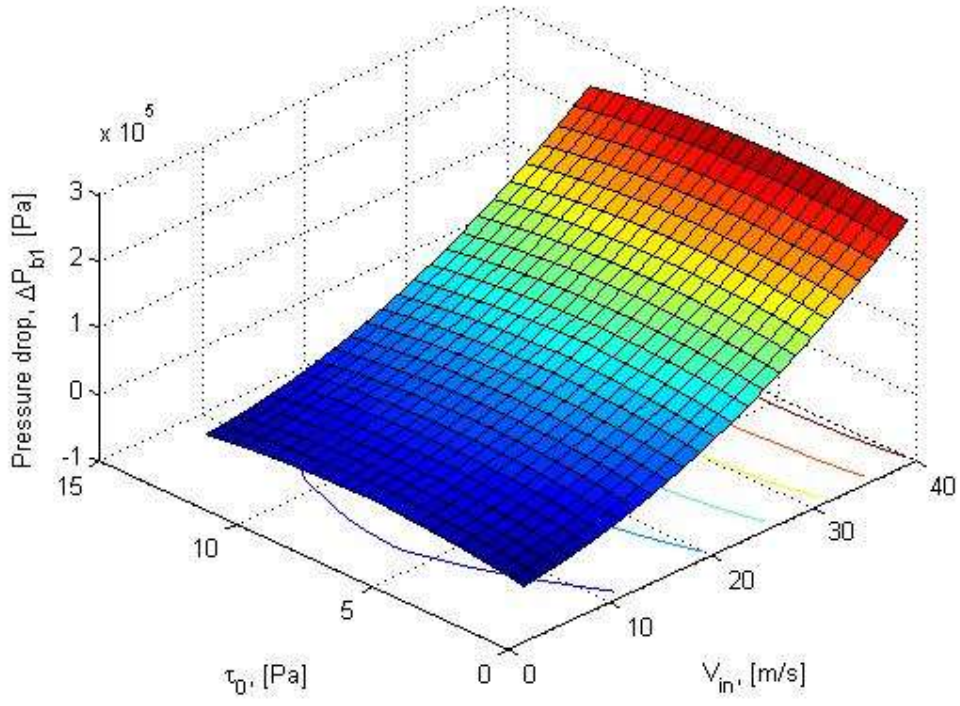

Figure 4.22: 3D Response Charts of ΔP_{b1} against τ_o against V_{in}.

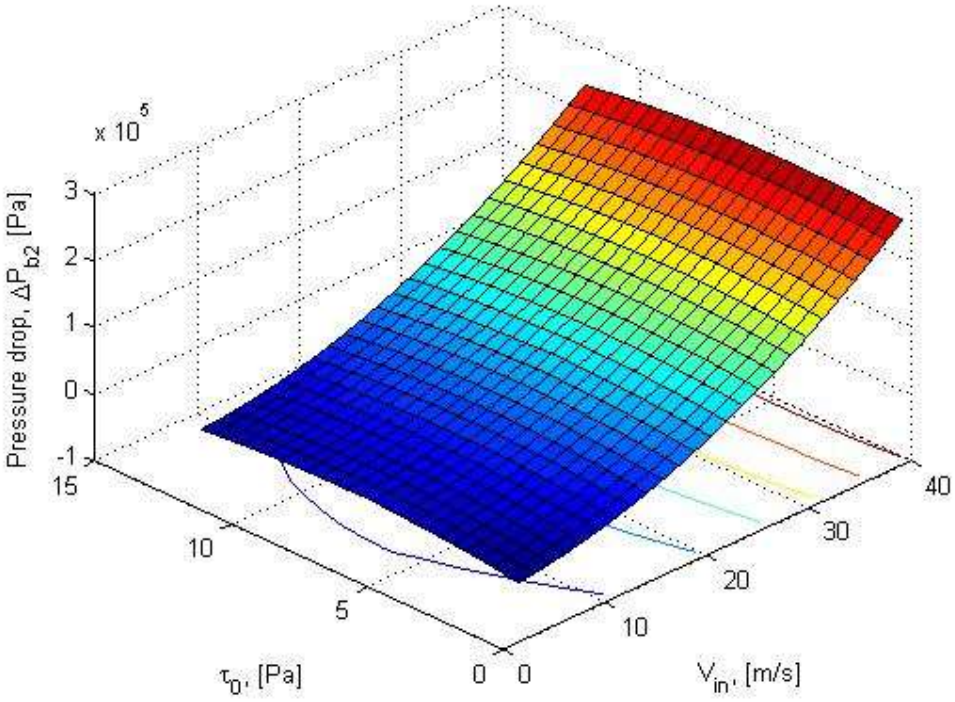

Figure 4.23: 3D Response Charts of ΔP_{b2} against τ_o against V_{in}.

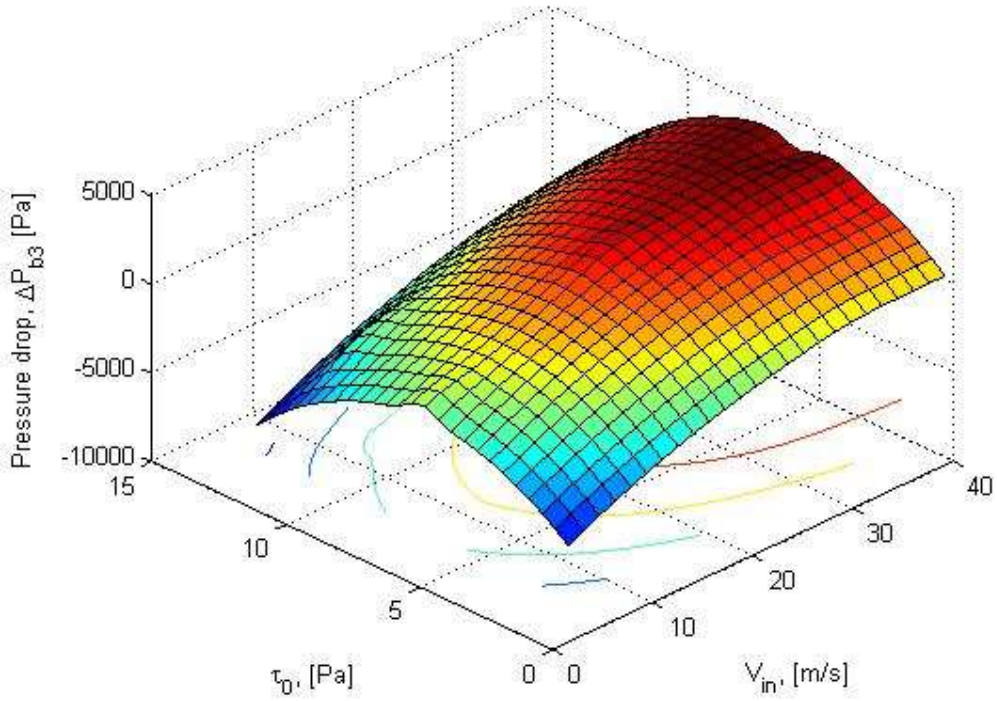

Figure 4.24: 3D Response Charts of ΔP_{b3} against τ_o against V_{in}.

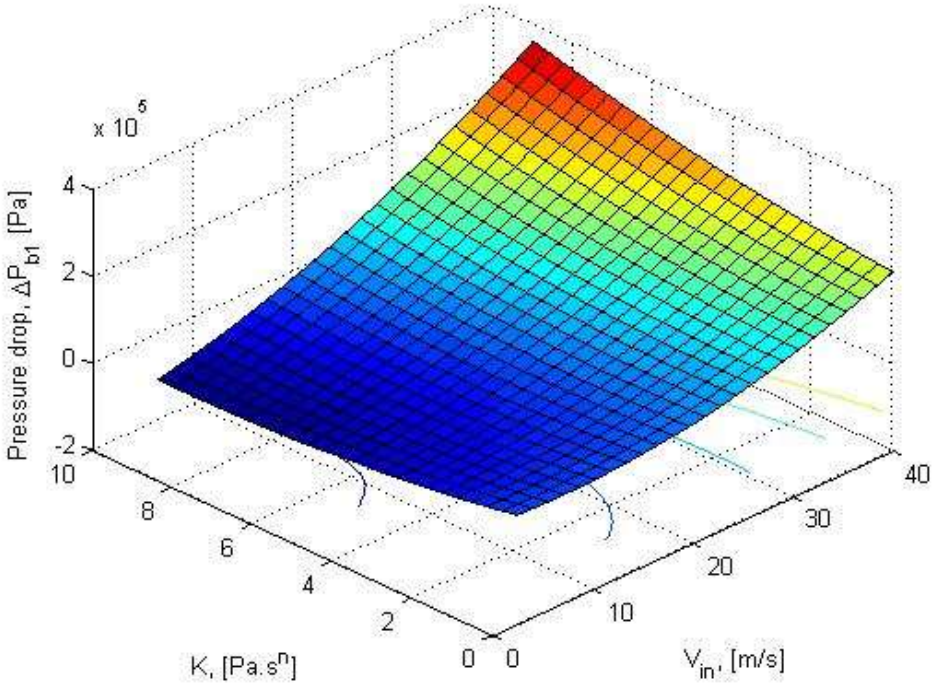

Figure 4.25: 3D Response Charts of ΔP_{b1} against K against V_{in}.

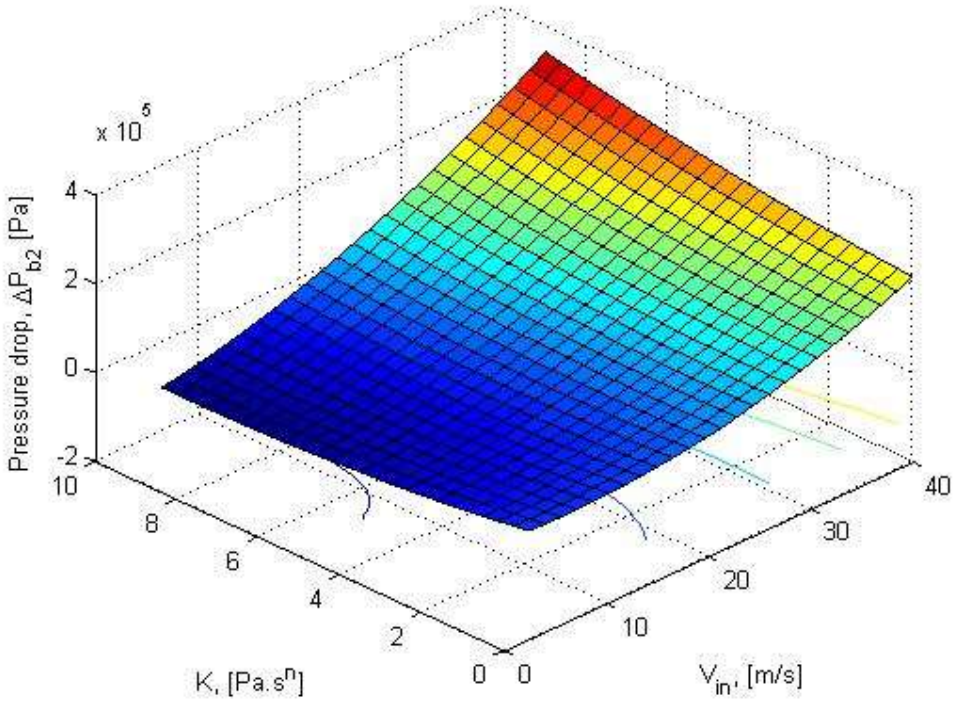

Figure 4.26: 3D Response Charts of ΔP_{b2} against K against V_{in}.

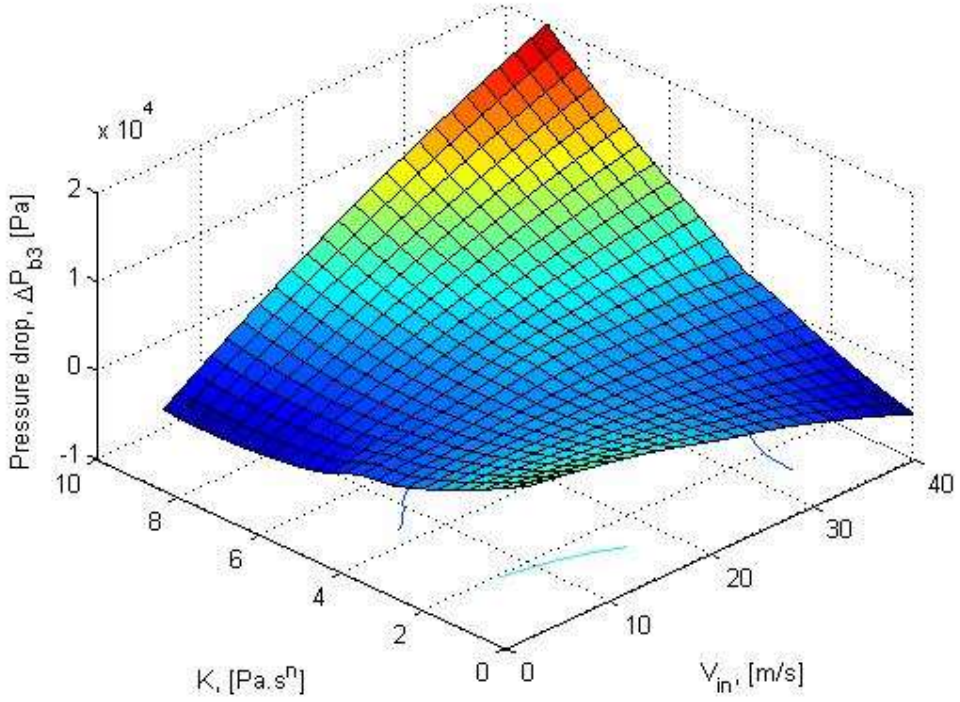

Figure 4.27: 3D Response Charts of ΔP_{b3} against K against V_{in}.

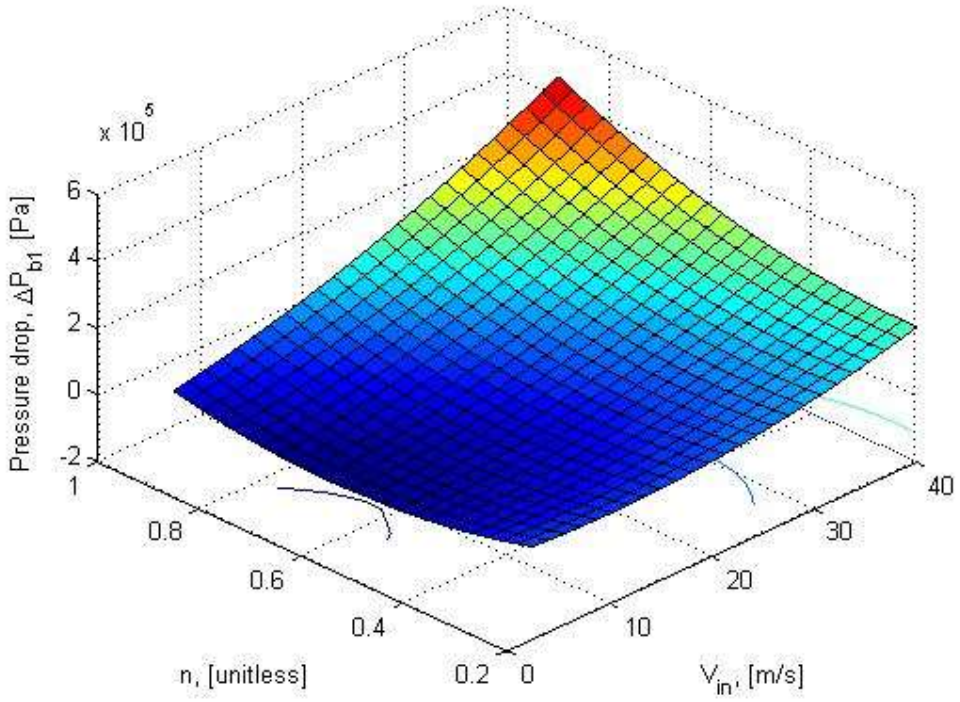

Figure 4.28: 3D Response Charts of ΔP_{b1} against n against V_{in}.

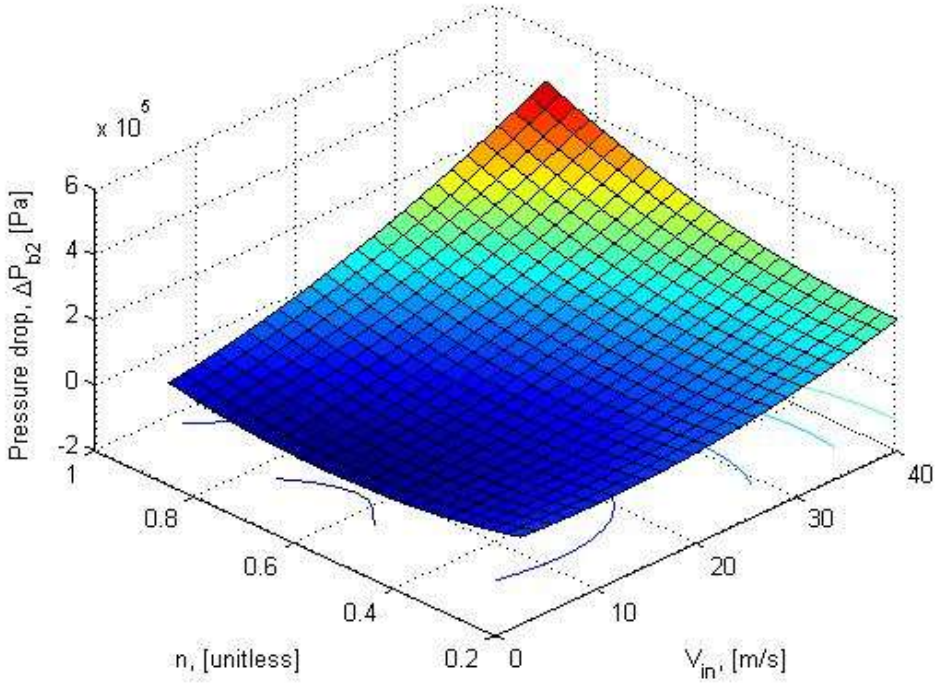

Figure 4.29: 3D Response Charts of ΔP_{b2} against n against V_{in}.

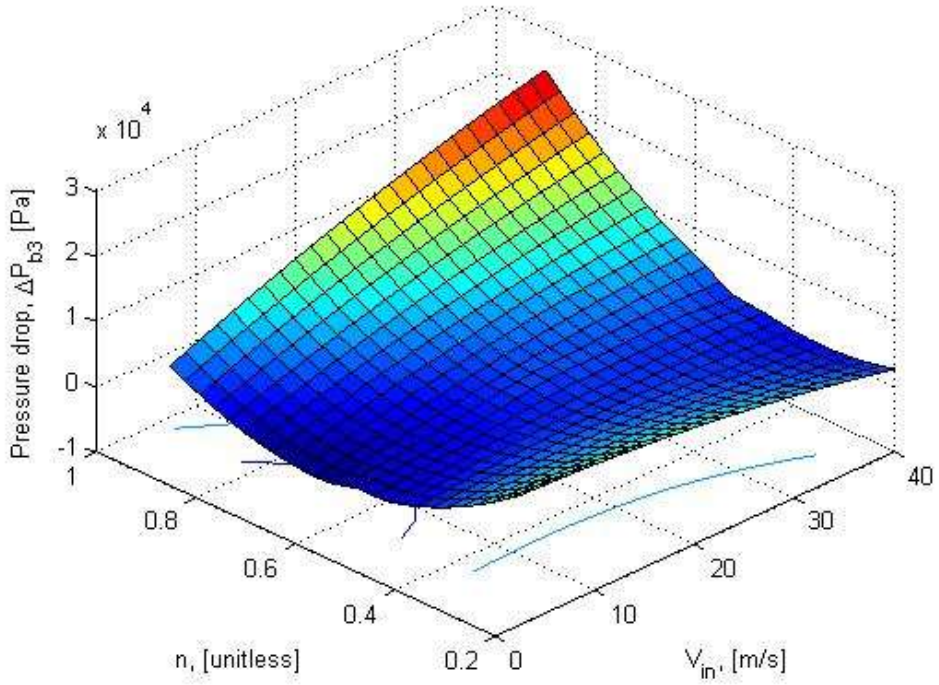

Figure 4.30: 3D Response Charts of ΔP_{b3} against n against V_{in}.

Based on the generated charts, there are unnoticeable or insignificant differences between ΔP_{b1} and $\Delta P_{b2.}$ This is because majority of pressure drop (Max pressure drop = 265759 Pa) occurs nearer to the PDC bit while minority of pressure drop (Max pressure drop = 13344 Pa) occurs away from the bit. Minor pressure drop is approximately 5% of the total pressure drop across the bit.

V_{in} and ΔP_b have the strongest correlation in all cases. Around the bit, ΔP_{b1} and ΔP_{b2} increases as V_{in} increases. However, away from the bit, ΔP_{b3} increases as V_{in} increases until 34 m/s and then ΔP_{b3} decreases. This shows that V_{in} has very strong positive effect on ΔP_b around the bit and slightly less effective away from the bit. To avoid large pressure drop across bit, flow velocity should be to a minimum 2.5 m/s.

τ_o and ΔP_b show the weak correlation in all cases. $\Delta P_{b1,}$ $\Delta P_{b2,}$ and ΔP_{b3} increase as τ_o increases. $\Delta P_{b1,}$ $\Delta P_{b2,}$ and ΔP_{b3} peak when τ_o is 5.6 Pa and then $\Delta P_{b1,}$ $\Delta P_{b2,}$ and ΔP_{b3} decrease as τ_o increases. τ_o has positive and negative effect on $\Delta P_{b1,}$ $\Delta P_{b2,}$ and $\Delta P_{b3.}$ The value of τ_o should be away from 5.6 Pa; either very small or large value. τ_o is better off at 11.25 Pa; the higher the better.

K and ΔP_b also show the moderate correlation in all cases. $\Delta P_{b1,}$ $\Delta P_{b2,}$ and ΔP_{b3} decrease slightly as K increases until 2.5 Pa.s^n and then $\Delta P_{b1,}$ $\Delta P_{b2,}$ and ΔP_{b3} increase as τ_o increases. To minimize pressure drop across bit, K value should be kept low; approximately 2.5 Pa.s^n.

n and ΔP_b show the strong correlation in all cases. ΔP_{b1} and ΔP_{b2} decrease slightly as n increases until n is 0.4 while ΔP_{b3} decreases slightly as increases until n is 0.45. After these points, $\Delta P_{b1,}$ $\Delta P_{b2,}$ and ΔP_{b3} increase as τ_o increases. To minimize pressure drop across bit, n value should be kept low; approximately 0.4.

Chapter 5: Conclusion and Recommendation

5.1 Conclusion

This research is about pressure drop across bit with respect to mud rheological parameters. Objectives were achieved with successful development of regression model of pressure drop across bit and optimization of parameters for improved ROP. Some important conclusions can be drawn as follows:

- Mud flow rate showed significant effect to pressure drop across the bit. The lower the inlet velocity, the lower the pressure drop.

- Mud rheology parameters have been proven to show moderate effects to pressure drop across the bit. Power Index showed significant effect to pressure drop. Consistency Index showed moderate effect while Yield Stress showed small effect to pressure drop.

- ROP is inversely proportional to the square root of pressure drop. The lower the pressure drop, the higher the ROP. This research has 4 input parameters and optimization analysis were done individually where the other 3 input parameters are kept at average values. Optimized parameters for reduction in pressure drop across bit and improvement in ROP:

    - Inlet Velocity, V_{in} = 2.5m/s
    - Yield Stress, τ_o = 11.25 Pa
    - Consistency Index, K = 2.5 Pa.s^n
    - Power Index, n = 0.4

- Simulation on mud rheology showed a reduction of about 50% in pressure drop across the bit as compared to existing models. Existing pressure drop models should be revised to include mud rheology parameters.

5.2 Recommendation

- Further research on the effect of drill bit rotation (RPM) and its effect on the mud behavior should be considered as it was not considered in previous study.
- Use a different design points sampling approach in Design of Experiment.
- Develop pressure drop model in terms of mud density, TFA, nozzle coefficient, flow rate, yield stress, consistency index, and power index.
- Tweak PDC bit geometry for improved mud flow and to prevent future stagnation regions and bit balling.
- Two Phase flow simulation.
- Consider the effect of different bit sizing to pressure drop across bit.

References

[1] A. T. Bourgoyne, *Applied drilling engineering*. Richardson, Tex.: Society of Petroleum Engineers (U.S.), 1991.

[2] D. Hankins, S. Salehi, and F. Karbalaei Saleh, "An Integrated Approach for Drilling Optimization Using Advanced Drilling Optimizer," *Journal of Petroleum Engineering,* vol. 2015, pp. 1-12, 2015.

[3] L. W. Lake, J. R. Fanchi, R. F. Mitchell, K. E. Arnold, J. D. Clegg, E. D. Holstein*, et al.*, *Petroleum engineering handbook*. Richardson, TX: Society of Petroleum Engineers, 2006.

[4] DrillingFormulas. (2014, 14th October 2014). *What You Need To Know About Drilling Bit Balling Up and How To Troubleshooting It*. Available: http://www.drillingformulas.com/what-you-need-to-know-about-drilling-bit-balling-up-and-how-to-troubleshooting-it/

[5] I. Baker Hughes, "IADC Dull Grading System for Fixed Cutter Bits," in *Advancing Reservoir Performance*, ed, 2012.

[6] R. Black Gold. (2015). *Oil And Gas Well Directional Drilling*. Available: http://www.blackgoldresourcesinc.com/oil-and-gas-technology/#.VlMu2fkrKUk

[7] H. A. Kendall and W. C. Goins, Jr., "Design and Operation of Jet-Bit Programs For Maximum Hydraulic Horsepower, Impact Force or Jet Velocity," ed: Society of Petroleum Engineers, 1960.

[8] B. Guo and G. Liu. (2011). *Applied Drilling Circulation Systems: Hydraulics, Calculations and Models*.

[9] S. M. Hussaini and J. J. Azar, "Experimental Study of Drilled Cuttings Transport Using Common Drilling Muds," *Society of Petroleum Engineers Journal,* vol. 23, pp. 11-20, 1983/2/1/ 1983.

[10] P. H. Tomren, A. W. Iyoho, and J. J. Azar, "Experimental Study of Cuttings Transport in Directional Wells," *SPE Drilling Engineering,* vol. 1, pp. 43-56, 1986/2/1/ 1986.

[11] J. Li and S. Walker, "Sensitivity Analysis of Hole Cleaning Parameters in Directional Wells," 1991.

[12] H. Cho, S. N. Shah, and S. O. Osisanya, "Effects of Fluid Flow in a Porous Cuttings-Bed on Cuttings Transport Efficiency and Hydraulics," 2001.

[13] K. Ravi and T. Hemphill, "Pipe Rotation and Hole Cleaning in Eccentric Annulus," 2006.

[14] K. M. Lim and G. A. Chukwu, "Bit Hydraulics Analysis for Efficient Hole Cleaning," 1996.

[15] G. Mensa-Wilmot and M. Fear, "Innovative Technology Improves Penetration Rates of PDC Bits in Shales Drilled at Great Depth With Weighted Water Based Mud Systems," 2002.

[16] M. Wells, T. Marvel, and C. Beuershausen, "Bit Balling Mitigation in PDC Bit Design," 2008.

[17] A. Moslemi and G. Ahmadi, "Study of the Hydraulic Performance of Drill Bits Using a Computational Particle-Tracking Method," *Spe Drilling and Completion,* vol. 29, pp. 28-35, 2014.

[18] L. Robinson, "Drill Bit Nozzle Pressure Loss [Exploitation of Finagle Factor Technology]," *American Association of Drilling Engineers,* vol. AADE-10-DF-HO-26, pp. 1-9, 6 April 2010 2010.

[19] W. C. Lyons, "Chapter 4 - Drilling and Well Completions A2," in *Standard Handbook of Petroleum and Natural Gas Engineering (Third Edition)*, G. J. Plisga and M. D. Lorenz, Eds., ed Boston: Gulf Professional Publishing, 2016, pp. 4-1-4-584.

[20] T. Nazari, G. Hareland, and J. J. Azar, "Review of Cuttings Transport in Directional Well Drilling: Systematic Approach," 2010.

[21] M. E. Hossain and A. A. Al-Majed. (2015). *Fundamentals of sustainable drilling engineering*.

[22] R. Darby, "Viscoelastic Fluids. An Introduction to Their Properties and Behavior.," *Marcel Dekker,* vol. Volume 9, 1976.

[23] P. Skalle, *Drilling Fluid Engineering*, Third Edition ed.: Ventus Publishing ApS, 2012.

[24] I. Sandvold, "Gel Evolution in Oil Based Drilling Fluids," ed: Institutt for petroleumsteknologi og anvendt geofysikk, 2012, p. 129.

[25] J. Adachi, L. Bailey, O. H. Houwen, G. H. Meeten, P. W. Way, F. B. Growcock*, et al.*, "Depleted Zone Drilling: Reducing Mud Losses Into Fractures," 2004.

[26] Z. Chen, "Study of Cuttings Transport with Foam under Elevated Pressure and Elevated Temperature Conditions," November 14 - 15, 2005 2005.

[27] K. Simon, "The Role of Different Rheological Models In Accuracy Of Pressure Loss Prediction.," *Rudarsko-geološko-naftni zbornik* vol. Vol. 16, pp. 85-89 2004.

[28] H. H. Doiron and J. D. Deane, "Effects of Hydraulic Parameter Cleaning Variations on Rate of Penetration of Soft Formation Insert Bits," 1982.

[29] T. M. Warren and W. J. Winters, "The Effect of Nozzle Diameter on Jet Impact for a Tricone Bit," *Society of Petroleum Engineers Journal,* vol. 24, pp. 9-18, 1984/2/1/ 1984.

[30] T. M. Warren, "Penetration Rate Performance of Roller Cone Bits," *SPE Drilling Engineering,* vol. 2, pp. 9-18, 1987/3/1/ 1987.

[31] A. Wu, G. Hareland, B. Rashidi, X. Gao, and Y. Yang, "Geometrical Modeling of Rock Breakage Craters to Improve the Performance of a ROP Simulator," 2011.

[32] I. King, C. Bratu, B. Delbast, A. Besson, and J. P. Chabard, "Hydraulic Optimization of PDC Bits," 1990.

[33] W. Zhenquan and S. Dongyu, "Optimal Design of the Flow Field of Bi-center Bit," *Procedia Engineering,* vol. 73, pp. 345-351, 2014.

[34] ANSYS, "Using Design Exploration," in *Design Exploration User's Guide*, Release 12.1 ed, 2009, pp. 23-78.

[35] R. Monicard, "Drilling Mud and Cement Slurry Rheology Manual," 1982.

[36] M. S. R. Ramsey, L. H., "Onsite Continuous Hydraulics Optimization (OCHO™)," *AADE 2001 National Drilling Conference, Houston,* March 27-29, 2001 2001.

[37] T. M. Warren, "Evaluation of Jet-Bit Pressure Losses," 1989/12/1/.

[38] T. Hemphill, W. Campos, and A. Pilehvari, "Yield-Power Law Model More Accurately Predicts Mud Rheology," *Oil and Gas Journal,* vol. 91, August 23, 1993 1993.

[39] D. Glowka, "Optimization of Bit Hydraulic Configurations," *Society of Petroleum Engineers Journal,* vol. 23, pp. 21-32, 1983/2/1/ 2013.

Appendices

Table A1: Rheological Models of Fluid

Model	Equations	Source
Newtonian	$\tau = \mu \dot{\gamma}$	[1]
Power law	$\tau = k \dot{\gamma}^n$	[1]
Bingham plastic	$\tau = \tau_y + \mu_p \dot{\gamma}$	[1]
Yield Power Law (Herschel-Bulkley)	$\tau = \tau_y + k \dot{\gamma}^n$	[38]

Table A2: Compilation of previous studies on Pressure Drop Models.

Description	Equations	Source
C_d = 0.8 (Conventional Bit) C_d = 0.95 (Jet Bit)	$\Delta P_b = \frac{(MW)(Q^2)}{11884(C_d{}^2)(TFA^2)}$	[35]
C_d = 1.03	$\Delta P_b = \frac{(MW)(Q^2)}{12032(C_d{}^2)(TFA^2)}$	[18, 36, 37]
ROP and RPM	$\Delta P_b = \frac{(MW)(Q^2)}{8795[(TFA)(e^{-0.832})(\frac{ROP}{RPM})]^2}$	[19]

Table A3: Literature Review Summary

Parameter	Reported observation	Source
PDC Bit Hydraulics on C_t	<u>Effective factors toward C_t:</u> - HSI: Higher the better. And it leads to higher ROP and Nozzle-jet Velocity. Between HSI of 1.18hp/in^2 to 3.74hp/in^2, ROP increased by 37%,	[17]

	Nozzle-jet velocity increased by 77%, and C_t increased by 15%. Smaller nozzles provide higher HSI due to greater pressure drop. <u>Non-effective factors toward C_t:</u> - Number of Nozzles: For same TFA, lesser the better. Flow rate deviation is 30% for 7 nozzles while 20% for 5 nozzles. Imbalanced flow-rate distribution for 7 nozzles. - Nozzle Size: Smaller the better. - Nozzle Arrangement: No effect. - Waterway Profile: Flat is slightly better than Parabolic Profile. - Particle Size: Smaller the better. Sweet spot between 0.5mm to 1.0mm - Number of Released Particles: Higher the better.	
PDC Bit Hydraulics	<u>Effective factors:</u> - Nozzle Position: Closer to blades brings more significant fluid circulation. - Nozzle Inclination: 30° is better than 11° because 30° leads to higher velocity. - Nozzle Orientation: Parallel to channel axis has highest risk to bit balling. Azimuthal orientation (Parallel to blade) favors blade cleaning. - Nozzle Size: Bigger nozzle's wide spread of jet impact along blade is more important compared to smaller nozzle. However, eddies for smaller nozzle is	[32]

	located higher and farther from the bit surface. - Blade Curvature: Curved blades are better at cleaning than straight blades due to curved design avoids the important weak flow rate zones of blades. <u>Non-effective factors:</u> - Flow Rate: No effect to the overall flow behavior.	
PDC Bit Nozzles Configurations Through Experimental Setup	<u>Effective configuration:</u> - When only near bit center nozzles are open, there are higher flow velocities and generally a better cooling pattern across the bit face and bit is at much lower risk of bit balling due to favorable cuttings removal away from PDC bit. <u>Non-effective Configurations:</u> - When only away from bit center nozzles are open, there are unbalanced cooling of cutters (some are cooled better than others) and has potential problems at removing cuttings since there is a stagnation zone at the center of bit. Noted low pressure gradients that indicates poor cuttings removal away from PDC bit. - When all nozzles are open, flow velocities and heat transfer coefficients are lower than other configurations.	[39]
Effect of PDC Drilling Parameters to ROP	<u>Effective parameters to ROP:</u> - Bit Size: Smaller the better (significantly).	[2]

	- WOB: Bigger the better (significantly). - RPM: Bigger the better (significantly). - HHPb: Bigger the better (significantly). - Nozzle Size: Smaller the better (significantly). - Flow Rate: Bigger the better (significantly). - Mud Weight: Smaller the better (Significantly). - Number of Cutters: Smaller the better. - Back Rack Angle: Smaller the better. - Junk Slot Area: Bigger the better. <u>Non-effective parameters to ROP:</u> - Slide Rake Angle: No effect. - Plastic Viscosity: No effect.	